A&A 618, A16 (2018)
https://doi.org/10.1051/0004-6361/201832852

Astronomy & Astrophysics

3D non-LTE corrections for Li abundance and ^{6}Li/^{7}Li isotopic ratio in solar-type stars⋆

I. Application to HD 207129 and HD 95456

G. Harutyunyan[1], M. Steffen[1], A. Mott[1], E. Caffau[2], G. Israelian[3], J. I. González Hernández[3], and K. G. Strassmeier[1]

[1] Leibniz-Institut für Astrophysik Potsdam, An der Sternwarte 16, 14482 Potsdam, Germany
e-mail: gharutyunyan@aip.de
[2] GEPI, Observatoire de Paris, PSL Research University, CNRS, Univ. Paris Diderot, Sorbonne Paris Cité, Place Jules Janssen, 92190 Meudon, France
[3] Instituto de Astrofísica de Canarias, 38200 La Laguna, Tenerife, Spain

Received 19 February 2018 / Accepted 29 June 2018

ABSTRACT

Context. Convective motions in solar-type stellar atmospheres induce Doppler shifts that affect the strengths and shapes of spectral absorption lines and create slightly asymmetric line profiles. One-dimensional (1D) local thermodynamic equilibrium (LTE) studies of elemental abundances are not able to reproduce this phenomenon, which becomes particularly important when modeling the impact of isotopic fine structure, like the subtle depression created by the ^{6}Li isotope on the red wing of the Li I resonance doublet line.
Aims. The purpose of this work is to provide corrections for the lithium abundance, A(Li), and the ^{6}Li/^{7}Li isotopic ratio that can easily be applied to correct 1D LTE lithium abundances in G and F dwarf stars of approximately solar mass and metallicity for three-dimensional (3D) and non-LTE (NLTE) effects.
Methods. The corrections for A(Li) and ^{6}Li/^{7}Li are computed using grids of 3D NLTE and 1D LTE synthetic lithium line profiles, generated from 3D hydro-dynamical CO^{5}BOLD and 1D hydrostatic model atmospheres, respectively. For comparative purposes, all calculations are performed for three different line lists representing the Li I λ670.8 nm spectral region. The 3D NLTE corrections are then approximated by analytical expressions as a function of the stellar parameters ($T_{\rm eff}$, $\log g$, [Fe/H], $v \sin i$, A(Li), ^{6}Li/^{7}Li). These are applied to adjust the 1D LTE isotopic lithium abundances in two solar-type stars, HD 207129 and HD 95456, for which high-quality HARPS observations are available.
Results. The derived 3D NLTE corrections range between −0.01 and +0.11 dex for A(Li), and between −4.9 and −0.4% for ^{6}Li/^{7}Li, depending on the adopted stellar parameters. We confirm that the inferred ^{6}Li abundance depends critically on the strength of the Si I 670.8025 nm line. Our findings show a general consistency with recent works on lithium abundance corrections. After the application of such corrections, we do not find a significant amount of ^{6}Li in any of the two target stars.
Conclusions. In the case of ^{6}Li/^{7}Li, our corrections are always negative, showing that 1D LTE analysis can significantly overestimate the presence of ^{6}Li (up to 4.9% points) in the atmospheres of solar-like dwarf stars. These results emphasize the importance of reliable 3D model atmospheres combined with NLTE line formation for deriving precise isotopic lithium abundances. Although 3D NLTE spectral synthesis implies an extensive computational effort, the results can be made accessible with parametric tools like the ones presented in this work.

Key words. stars: abundances – stars: atmospheres – radiative transfer – line: formation – line: profiles

1. Introduction

The lithium abundance, A(Li)[1], and the ^{6}Li/^{7}Li isotopic ratio measured in stellar atmospheres can provide valuable information contributing to understanding different problems in astrophysics such as stellar structure and evolution, stellar activity, exoplanetary system evolution and even cosmology. A reliable determination of the lithium content in stellar atmospheres is important, and apart from requiring high-resolution stellar spectra with high signal-to-noise ratios (S/Ns), it also requires realistic stellar atmosphere models allowing a sound theoretical interpretation of both the strength and the shape of the Li lines.

The stable isotope ^{7}Li is among the few light elements that have been produced in the Big Bang. In contrast, the other stable isotope, ^{6}Li, is not produced in significant amounts in standard Big Bang nucleosynthesis (e.g., Thomas et al. 1993), but mainly through spallation and $\alpha + \alpha$ fusion reactions triggered by high-energy collisions between Galactic cosmic rays and He, C, N, O nuclei in the interstellar medium (e.g., Meneguzzi et al. 1971; Prantzos et al. 1993; Prantzos 2012). Additional ^{7}Li is produced by the same mechanism, and partly by stellar nucleosynthesis as well. The current ^{6}Li/^{7}Li in the local interstellar medium (ISM) is measured to be ∼13% (Kawanomoto et al. 2009, see also Howk et al. 2012), while the solar system (meteoritic) ^{6}Li/^{7}Li is 8.2% (Lodders 2003).

Both ^{6}Li and ^{7}Li are very fragile with respect to nuclear reactions with protons and are destroyed in stellar interiors at temperatures above ∼2.0×10^6 K and ∼2.5×10^6 K, respectively (e.g., Pinsonneault 1997). According to standard stellar

⋆ The table with the 3D NLTE corrections is only available at the CDS via anonymous ftp to cdsarc.u-strasbg.fr (130.79.128.5) or via http://cdsarc.u-strasbg.fr/viz-bin/qcat?J/A+A/618/A16

[1] A(X) = log(N(X)/N(H)) + 12, where X is the chemical element.

evolution models, ^{6}Li, being the more fragile of the two isotopes, undergoes an intense destruction during pre-main sequence evolution (e.g., Forestini 1994; Proffitt & Michaud 1989; Montalbán & Rebolo 2002). The standard models predict that by the time a solar-type solar-metallicity star reaches the main sequence its ^{6}Li has already been destroyed by nuclear reactions at the base of the extended, completely mixed convective envelope. In non-standard stellar evolution, where additional processes such as rotational mixing, atomic diffusion, internal gravity waves, and the effect of magnetic fields are included in order to explain the observed lithium abundances in stellar atmospheres (see Talon & Charbonnel 2005 and references therein), lithium destruction is generally even enhanced compared to the standard models.

This suggests that any significant detection of the fragile ^{6}Li isotope in the atmosphere of a solar-type star would most probably indicate an external pollution process, for example by planetary matter accretion (Israelian et al. 2001) or alternative sources like stellar flares (Montes & Ramsey 1998). ^{6}Li can also be produced by superflares around stars with hot Jupiters (Cuntz et al. 2000). Therefore, it is of great interest to measure the presence of the ^{6}Li isotope in solar-type stars with effective temperatures between 5900 and 6400 K (see Montalbán & Rebolo 2002) and, in case of a positive detection, to investigate its origin.

Israelian et al. (2001) measured ^{6}Li/^{7}Li in the giant-planet hosting star HD 82943 and found a significant amount of ^{6}Li in its atmosphere (^{6}Li/^{7}Li = 12%, reduced to 5% after being remeasured by Israelian et al. 2003). This finding was interpreted as evidence for a planetary material accretion on the surface of the star. ^{6}Li/^{7}Li has been measured afterwards by several other groups in small samples of main-sequence solar-metallicity stars with and without known planets (Reddy et al. 2002; Mandell et al. 2004; Ghezzi et al. 2009; Pavlenko et al. 2018), but no significant detections of ^{6}Li have been reported.

The use of one-dimensional (1D) model atmospheres can lead to erroneous results in terms of lithium isotopic ratios, due to the fact that the missing convective line asymmetry must be compensated by a spurious ^{6}Li abundance to fit the observed line profile. The result is an overestimation of ^{6}Li/^{7}Li using 1D model atmospheres (e.g., Cayrel et al. 2007, Steffen et al. 2012). Furthermore, not only Li but also all other spectral lines have asymmetric profiles. The asymmetry depends on several factors such as the mean depth of formation and atomic mass. The use of detailed three-dimensional (3D) hydrodynamical model atmospheres allows us to obtain more reliable abundances and isotopic ratios, in particular since they are able to treat the convective motions responsible for the line asymmetries in a much more realistic way compared to standard 1D model atmospheres. In addition, in the case of lithium, the line formation must be treated considering departures from local thermodynamic equilibrium (LTE) that are known to be significant, especially in metal-poor stars (Cayrel et al. 2007), affecting not only the strength of the spectral line but also its Doppler shift.

On the other hand, 3D non-LTE (NLTE) calculations are computationally demanding and not easily accessible to the scientific community. For this reason, it is important to provide some simplified approach to correct the results of any 1D LTE spectral analysis of the lithium line region for both 3D and NLTE effects. Such an approach was suggested by Steffen et al. (2010a,b, 2012). In Steffen et al. (2012), the authors used a grid of 3D model atmospheres to derive a polynomial approximation for deriving the 3D NLTE correction of ^{6}Li/^{7}Li as a function of $T_{\rm eff}$, $\log g$ and metallicity ([Fe/H] from −3 to 0).

A similar approach was followed by Sbordone et al. (2010) for the lithium abundance. They derived analytical approximations to convert the equivalent widths (EW) of the lithium 670.8 nm line into A(Li) (and vice versa) in 1D LTE, 1D NLTE and 3D NLTE, which, in principle, can be used to infer the 3D NLTE abundance correction by comparing the 1D LTE and 3D NLTE A(Li) for a given EW, $T_{\rm eff}$, $\log g$ and [Fe/H].

Several authors have previously performed 1D NLTE analyses of A(Li), covering a large range of stellar parameters (e.g., Carlsson et al. 1994, Pavlenko & Magazzu 1996, Takeda & Kawanomoto 2005, Lind et al. 2009). We compare our 3D NLTE and 1D NLTE results with some of the previous works in Sect. 2.6. In the context of very metal-poor stars, where no blend lines interfere, the most advanced full 3D NLTE analyses of ^{6}Li/^{7}Li have been performed by Lind et al. (2013), who showed that previous detections of ^{6}Li based on 1D and 3D LTE modeling could not be confirmed when reanalyzed with refined 3D NLTE methods. On the other hand, Mott et al. (2017) found clear evidence for the presence of ^{6}Li in the active subgiant HD 123351, both in 1D LTE and in a full 3D non-LTE analysis of very-high-quality spectra. Since the latter investigations use dedicated 3D model atmospheres to analyze individual stars, they do not provide a systematic grid of isotopic abundance corrections.

In this work, we use a grid of synthetic spectra computed from 3D hydrodynamical CO^{5}BOLD models and 1D hydrostatic LHD model atmospheres for a typical range of stellar parameters for solar-type stars. The intention is to provide a set of 3D NLTE corrections for the lithium abundance, A(Li), and in particular for ^{6}Li/^{7}Li that can be directly used to correct the results of 1D LTE analyses.

The ultimate purpose of this work is to facilitate the analysis of high-resolution and high-S/N spectra of a large sample of solar-type stars with and without known giant planets. In case of any positive detection of the fragile ^{6}Li isotope in the atmosphere of our target stars, we aim to investigate its possible source (e.g., planetary material accretion, flare production, etc.) by looking for correlations between the derived lithium content and the presence of a giant planet or planetary system.

This manuscript consists of two major parts. In Sect. 2, the methods and the results of the computations of 3D NLTE corrections for A(Li) and ^{6}Li/^{7}Li are presented, and the analytical expressions for their quick evaluation are provided. Section 3 explains the analysis and gives the results for A(Li) and ^{6}Li/^{7}Li measurements in two solar-type stars, HD 95456 and HD 207129, using their HARPS spectra. A summary and our conclusions are presented in Sect. 4.

2. 3D NLTE corrections

2.1. Model atmospheres

For deriving our 3D NLTE corrections, we adopted a subset of the CIFIST 3D hydrodynamical model atmospheres grid (Ludwig et al. 2009), computed with the CO^{5}BOLD code (Freytag et al. 2002, 2012). In total, 24 3D model atmospheres were used, covering three different effective temperatures ($T_{\rm eff}$), two surface gravities ($\log g$) and four metallicities ([Fe/H]). Table 1 lists the assigned number of each model (Model N) and its effective temperature, surface gravity, metallicity, number of the representative snapshots ($N_{\rm snap}$), and the number of opacity bins ($N_{\rm bins}$) for treating the radiative energy transport in the 3D simulations. The final $T_{\rm eff}$ of each CO^{5}BOLD hydrodynamical model atmosphere is determined after the selection of a number

Table 1. CO^{5}BOLD 3D hydrodynamical model atmospheres used in this work.

Model N	$T_{\rm eff}$ (K)	$\log g$	[Fe/H]	$N_{\rm snap}$	$N_{\rm bins}$
1	5850	4.0	−1.0	20	6
2	5920	4.5	−1.0	8	6
3	6260	4.0	−1.0	20	6
4	6240	4.5	−1.0	20	6
5	6500	4.0	−1.0	20	6
6	6460	4.5	−1.0	19	6
7	5920	4.0	−0.5	20	6
8	5900	4.5	−0.5	20	6
9	6250	4.0	−0.5	20	6
10	6230	4.5	−0.5	20	6
11	6520	4.0	−0.5	20	6
12	6490	4.5	−0.5	20	6
13	5930	4.0	0.0	18	5
14	5870	4.5	0.0	19	5
15	6230	4.0	0.0	20	5
16	6230	4.5	0.0	20	5
17	6490	4.0	0.0	20	5
18	6460	4.5	0.0	20	5
19	5870	4.0	0.5	20	5
20	5900	4.5	0.5	20	5
21	6190	4.0	0.5	20	5
22	6350	4.5	0.5	20	5
23	6410	4.0	0.5	20	5
24	6390	4.5	0.5	20	5

Notes. $N_{\rm snap}$ is the number of selected representative snapshots, and $N_{\rm bins}$ is the number of opacity bins.

of snapshots from their averaged radiative surface flux (this $T_{\rm eff}$ is given in Table 1) and usually differs slightly from the intended $T_{\rm eff}$ value. Therefore, the model atmospheres in our grid do not have exactly the same effective temperatures for each nominal temperature point of the grid.

To each CO^{5}BOLD model in our grid a 1D LHD model atmosphere (Caffau et al. 2008) is associated, having the same effective temperature, metallicity, and surface gravity. Using these particular 1D model atmospheres for comparison with the 3D models is advantageous since they employ the same opacity tables and equation of state as the CO^{5}BOLD models. Such a differential analysis minimizes unphysical (numerical) intrinsic differences between 1D and 3D models and isolates the true 3D effects. The 1D LHD model atmospheres employ the mixing-length theory to describe convection, and a typical mixing length parameter $\alpha_{\rm MLT} = 1.0$ is used in this work. Several authors (e.g., Klevas et al. 2016; Mott et al. 2017) have shown (as verified in Sect. 2.4.2 below) that the choice of this parameter is not critical for our A(Li) and ^{6}Li/^{7}Li studies. This is because, in the framework of the mixing-length theory, the line-forming layers of the considered stellar atmospheres are not strongly affected by convection.

2.2. Spectral synthesis

For each 3D CO^{5}BOLD and 1D LHD model atmosphere, a corresponding grid of synthetic spectra for the Li I λ670.8 nm region has been computed using the spectral synthesis code Linfor3D (Steffen et al. 2015). The NLTE lithium line profiles for the 3D case were computed for combinations of three different Li abundances (A(Li)$_{\rm 3DNLTE}$ = 1.5, 2.0, 2.5) and three different ^{6}Li/^{7}Li isotopic ratios (q(Li)$_{\rm 3DNLTE}$ = 0%, 5%, 10%); hereafter q(Li) = $n(^6{\rm Li})/n(^7{\rm Li})$.

A 17-level lithium model atom including 34 bound-bound transitions was adopted for the computation of the NLTE departure coefficients. This model atom was initially developed by Cayrel et al. (2007) and further updated and used by several authors (e.g., Sbordone et al. 2010; Steffen et al. 2012; Klevas et al. 2016; Mott et al. 2017). Individually for each of the three assumed lithium abundances, NLTE departure coefficients were computed with the code NLTE3D (Steffen et al. 2015).

In the 1D case, a series of LTE synthetic line profiles were computed for combinations of nine Li abundance values (from 1.00 to 3.00 with a step of 0.25), nine different ^{6}Li/^{7}Li isotopic ratios (from 0% to 16% with a step of 2%), and three different microturbulence velocities ($V_{\rm micro}$), centered on the value obtained from the analytic expression derived from a set of 3D model atmospheres by Dutra-Ferreira et al. (2016), with an offset of ±0.5 kms^{-1}.

To examine the dependence of our results on the list of blend lines used in the spectral synthesis, we replicated the computation of the full grids of 3D NLTE and 1D LTE line profiles using three different line lists. The first line list includes only the Li I atomic lines adapted from Kurucz (1995). The original hyperfine structure was simplified to include six ^{6}Li and six ^{7}Li components (hereafter, K95; as given in Mott et al. 2017). The second line list was constructed by Ghezzi et al. (2009; hereafter, G09), including 31 blend lines in addition to Li, whereas the third line list with 36 additional blend lines has been taken from Meléndez et al. (2012; hereafter, M12). In the case of G09 and M12, we have replaced the Li I hyper-fine structure by the same data as in K95.

Moreover, to be able to distinguish between the contributions of 3D and NLTE effects in the combined 3D NLTE corrections, we computed 1D NLTE spectra with the same methods and for the same grid as the 3D NLTE spectra but only for A(Li)$_{\rm 1DNLTE}$ = 2.0 and ^{6}Li/^{7}Li$_{\rm 1DNLTE}$ = 5%, adopting the line list K95. The 1D NLTE spectra were computed using the 1D LHD model atmospheres together with NLTE departure coefficients computed with NLTE3D.

All the synthetic spectra are computed in the wavelength range between 670.69 and 670.87 nm for the K95 line list, and between 670.672 and 670.888 nm in case of line lists G09 and M12, to be able to include in the synthesized spectral region the blends other than lithium that are present in the line lists.

2.3. 3D–1D fitting procedure

At first we derived the 1D LTE lithium abundance and the ^{6}Li/^{7}Li isotopic ratio by fitting each 3D NLTE line profile with the grid of pre-computed 1D LTE spectra. This is done for each value of A(Li)$_{\rm 3DNLTE}$ and q(Li)$_{\rm 3DNLTE}$ of the 3D NLTE grid. All 3D spectra were broadened with a Gaussian instrumental profile of $FWHM$ = 3.0 km s^{-1}, a value close to the resolution of the HARPS spectrograph. The fitting was performed through interpolation within the 1D LTE grid, driven by the least-squares fitting algorithm MPFIT (Markwardt 2009). Four free parameters were varied to achieve the best fit (χ^2 minimization): A(Li), q(Li), the FWHM of the Gaussian line broadening, and a global wavelength shift (Δv). The Gaussian broadening accounts for instrumental broadening and macroturbulence velocity ($V_{\rm macro}$) in the 1D case.

In addition, to investigate the possible dependence of our results on the rotational broadening, we applied identical

rotational broadening to the 3D and 1D spectra, ranging from $v \sin i = 0$ to 6 km s^{-1} with a step of 2 km s^{-1}. The rotational broadening is applied using the flux convolution approximation, assuming a typical limb darkening coefficient of $\epsilon = 0.6$ (e.g., Gray 2005).

2.4. 3D NLTE corrections for A(Li) and ^{6}Li/^{7}Li

We define the 3D NLTE correction of the lithium abundance, $\Delta^* A_{\rm 3DNLTE-1DLTE}$, as the difference between the $A({\rm Li})_{\rm 3DNLTE}$ value assumed in the 3D NLTE synthesis and the A(Li) value obtained from the best 1D LTE fit to the 3D NLTE spectrum. Similarly, the 3D NLTE correction for the lithium isotopic ratio, $\Delta^* q_{\rm 3DNLTE-1DLTE}$, is defined as the difference between the assumed $^6{\rm Li}/^7{\rm Li}_{\rm 3DNLTE}$ of the 3D NLTE spectrum and the best-fitting 1D LTE ^{6}Li/^{7}Li value. The asterisk indicates that the corrections are computed on a grid of given 3D NLTE Li abundances.

2.4.1. Fitting the pure lithium feature

As an example, we show in Fig. 1 (top panel) the best fit to the pure lithium 3D NLTE spectrum achieved for $T_{\rm eff} = 5870$ K, $\log g = 4.5$, [Fe/H] = 0, $A({\rm Li})_{\rm 3DNLTE} = 2.0$ and $q({\rm Li})_{\rm 3DNLTE} = 5\,\%$, computed adopting the Li hyperfine components from the line list K95. The ^{6}Li/^{7}Li isotopic ratio obtained by the best 1D LTE fit is q(Li) = 6.1%, thus overestimating the true 3D NLTE ^{6}Li/^{7}Li of 5% by 1.1% points, and underestimating the lithium abundance by ~0.08 dex.

The 3D NLTE corrections ($\Delta^* A_{\rm 3DNLTE-1DLTE}$ and $\Delta^* q_{\rm 3DNLTE-1DLTE}$) are computed for a grid of three $A({\rm Li})_{\rm 3DNLTE}$ and three $q({\rm Li})_{\rm 3DNLTE}$ values for each 3D model atmosphere given in Table 1. These corrections are meant for correcting the 1D LTE results without knowing the 3D NLTE $A({\rm Li})_{\rm 3DNLTE}$ and $^6{\rm Li}/^7{\rm Li}_{\rm 3DNLTE}$ of the observed spectrum, and therefore, they should not depend on the 3D NLTE values of $A({\rm Li})_{\rm 3DNLTE}$ and $q({\rm Li})_{\rm 3DNLTE}$ but on the measured 1D LTE values. Therefore, we converted our 3D NLTE corrections such that they depend on the 1D LTE lithium abundance, A(Li), and 1D LTE isotopic ratio, q(Li), instead of depending on the true (3D NLTE) values $A({\rm Li})_{\rm 3DNLTE}$ and $q({\rm Li})_{\rm 3DNLTE}$. To do this, we used the best-fitting 1D LTE values of the lithium abundance and the ^{6}Li/^{7}Li isotopic ratio for each $A({\rm Li})_{\rm 3DNLTE}$ and $q({\rm Li})_{\rm 3DNLTE}$ point of our 3D NLTE grid and interpolated the 3D NLTE corrections to the 1D LTE values A(Li) = 1.5, 2.0, 2.5 and q(Li) = 0, 5 and 10%. All the subsequent plots and tables presented in this work will be using these 3D NLTE corrections as a function of A(Li) and q(Li), denoted as $\Delta A_{\rm 3DNLTE-1DLTE}$ and $\Delta q_{\rm 3DNLTE-1DLTE}$, respectively.

Figure 2 shows the 3D NLTE corrections plotted vs. $T_{\rm eff}$ for ^{6}Li/^{7}Li (upper left panel) and A(Li) (lower left panel) for [Fe/H] = 0, A(Li) = 2.0 and q(Li) = 5%. The corrections for surface gravities 4.0 and 4.5 are plotted as blue circles and red triangles, respectively, and are connected with lines of different style for different $v \sin i$ values. For a given $\log g$, the 3D NLTE corrections of ^{6}Li/^{7}Li ($\Delta q_{\rm 3DNLTE-1DLTE}$) become larger (more negative) for higher temperatures, and they are larger for the lower $\log g$. We note that $\Delta q_{\rm 3DNLTE-1DLTE}$ depends also on $v \sin i$, A(Li), and q(Li): for a given $\log g$ and $T_{\rm eff}$, they become smaller (more positive) for higher $v \sin i$, and for a given stellar parameters they will be higher for stars with higher lithium abundance and isotopic ratio. The dependence of $\Delta q_{\rm 3DNLTE-1DLTE}$ on the $V_{\rm micro}$ used for 1D LTE spectral synthesis is negligible, and we take the central value of $V_{\rm micro}$ as representative for this work.

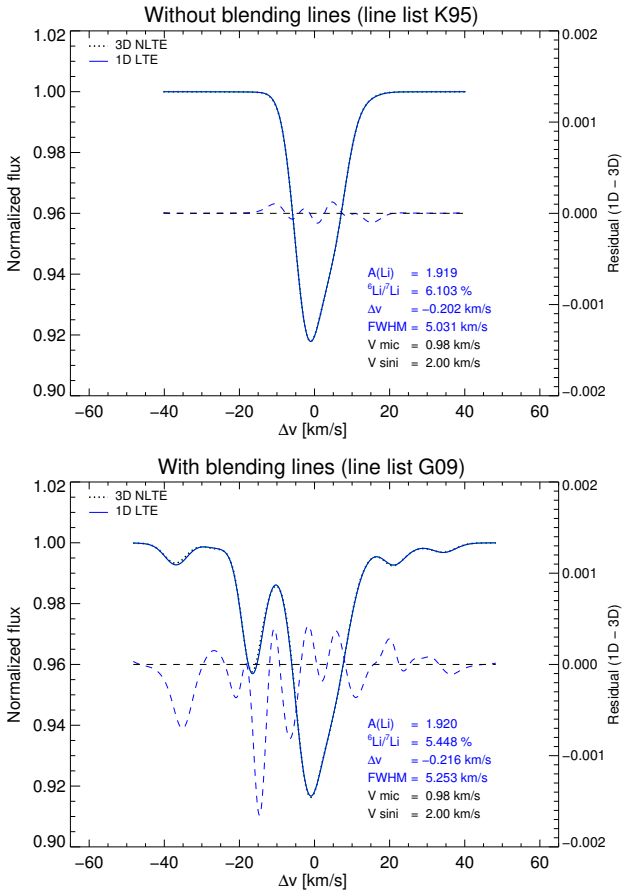

Fig. 1. The impact of the blending lines in the Li I λ670.8 nm region on the resulting 3D NLTE corrections. The best fitting 1D LTE spectrum (blue continuous line) is superimposed on the 3D NLTE spectrum (black dotted line) computed for $T_{\rm eff} = 5870$ K, $\log g = 4.5$, [Fe/H] = 0, $A({\rm Li})_{\rm 3DNLTE} = 2.0$, $^6{\rm Li}/^7{\rm Li}_{\rm 3DNLTE} = 5\%$ and representing the "observation". The synthetic spectra are computed adopting only the Li I doublet including hyperfine structure (line list K95, *upper panel*), and the line list G09 (*lower panel*), which includes also other atomic blends. The right y-axis gives the scale of the residuals (blue dashed line). We measure A(Li) = 1.92 and ^{6}Li/^{7}Li = 6.1% for line list K95, and A(Li) = 1.92 and ^{6}Li/^{7}Li = 5.4% in case of line list G09.

On the other hand, the 3D NLTE corrections for the lithium abundance, $\Delta A_{\rm 3DNLTE-1DLTE}$, become larger for lower effective temperatures. There is only a slight dependence on the surface gravity, and their dependence on the $v \sin i$ can be neglected (see Fig. 2, lower left panel). The $\Delta A_{\rm 3DNLTE-1DLTE}$ corrections do not show variations for different $V_{\rm micro}$ and q(Li) values, whereas they are decreasing slightly with larger A(Li) values.

Similar plots for the other three metallicities of our grid are given in Appendix A. For full details, we provide electronically a table of the corrections for $T_{\rm eff} = 5900$, 6300, 6500 K, $\log g = 4.0$ and 4.5, [Fe/H] = −1.0, −0.5, 0.0, 0.5, A(Li) = 1.5, 2.0, 2.5, q(Li) = 0, 5, 10%, and $v \sin i = 0.0$, 2.0, 4.0, 6.0 km s^{-1}, based on the pure lithium line list K95.

2.4.2. The impact of the mixing-length parameter

To investigate the dependence of our results on the choice of the mixing length parameter for 1D LHD models, we computed $\Delta A_{\rm 3DNLTE-1DLTE}$ and $\Delta q_{\rm 3DNLTE-1DLTE}$ using the models N 1–6 and N 13–18 with $\alpha_{\rm MLT} = 0.5$ and 1.5 (N 3, 15 and 17 only with $\alpha_{\rm MLT} = 0.5$). As expected, the choice of this parameter did not

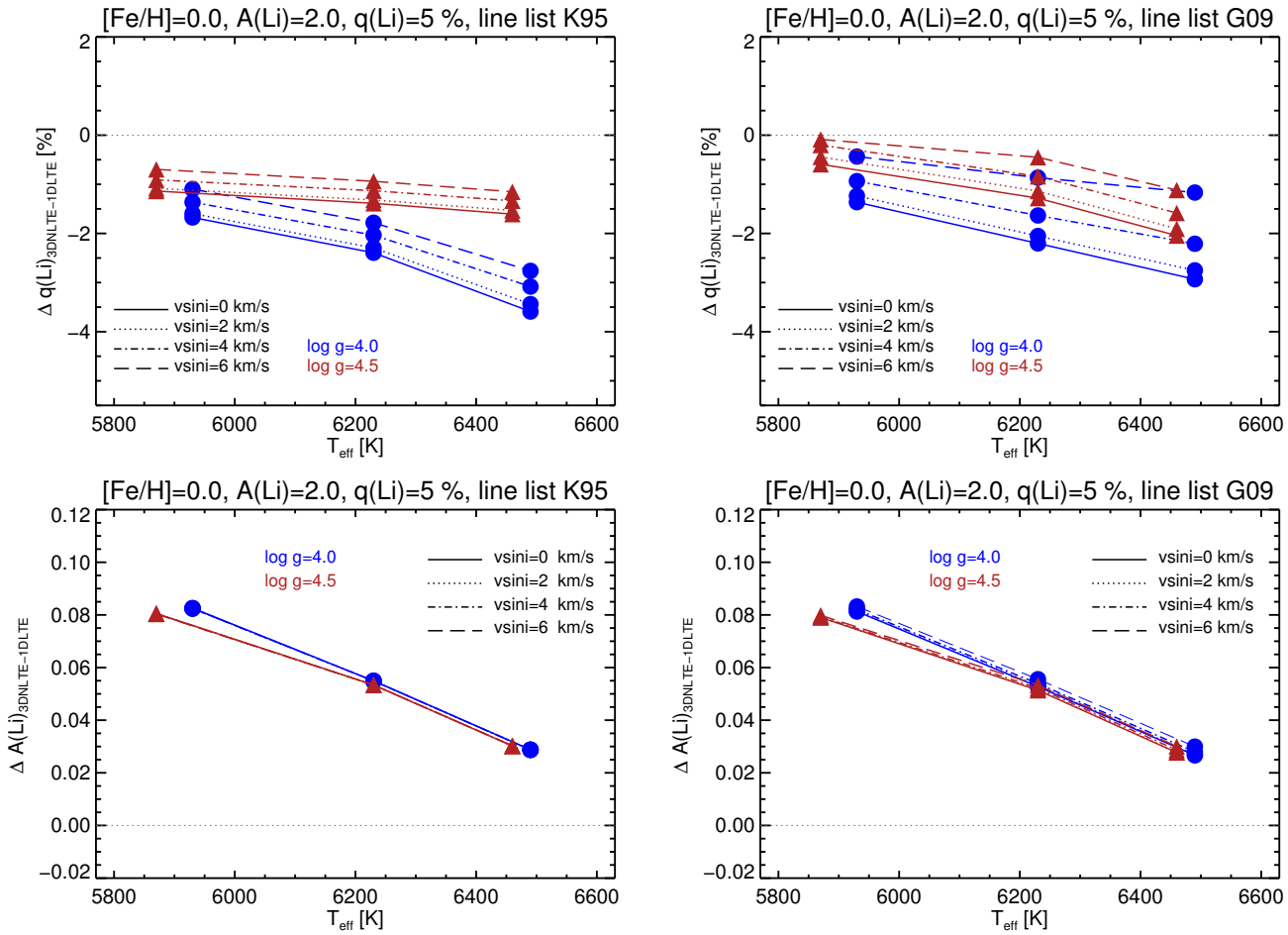

Fig. 2. 3D NLTE corrections $\Delta q_{\,3\mathrm{DNLTE-1DLTE}}$ (*upper panels*) and $\Delta A_{\,3\mathrm{DNLTE-1DLTE}}$ (*lower panels*) vs. $T_{\rm eff}$ for [Fe/H] = 0, A(Li) = 2.0, q(Li) = 5%, obtained with line lists K95 (*left panels*) and G09 (*right panels*). The blue circles and the red triangles correspond to $\log g = 4.0$ and $\log g = 4.5$, respectively. The computed 3D NLTE corrections for different $v \sin i$ values are connected with lines of different styles (see legend).

affect the $\Delta q_{\,3\mathrm{DNLTE-1DLTE}}$ results, while $\Delta A_{\,3\mathrm{DNLTE-1DLTE}}$ varied slightly by ±0.01 dex over the considered range of $\alpha_{\rm MLT}$.

2.4.3. The impact of blend lines

The bottom panel of Fig. 1 shows the best fit to the 3D NLTE spectrum computed for the same parameters as in Sect. 2.4.1, but now adopting line list G09 that includes atomic and molecular blends partly overlapping with the Li feature. In this case, the 3D NLTE correction of the ^{6}Li/^{7}Li isotopic ratio is somewhat smaller (−0.45% points), while the 3D NLTE correction for A(Li) is similar to the K95 case (∼+0.08 dex).

Initially, we were expecting that the fitting results would depend only weakly on the adopted line list. Comparison of the lower panels of Fig. 2 shows that this is basically the case for the A(Li) correction. However, while the ^{6}Li/^{7}Li corrections derived with line list G09 are qualitatively similar to those obtained from fitting the pure lithium spectrum, there are quantitative differences that depend on a variety of factors.

As shown in Fig. 1 (bottom), the blends in this spectral region may be quite strong (e.g., the Fe I line at ∼670.74 nm) and can play an even greater role in the fitting procedure than the Li I line itself. We recall that the main fitting parameters are A(Li) and q(Li), both only influencing the Li line, while the two remaining fitting parameters, global Gaussian line broadening and line shift, act on the all spectral lines. However, to keep the dimensionality of the problem manageable, the strength and wavelength shift of the individual blend lines is not adjusted in the fitting procedure. This deficiency of our method can lead to meaningless fitting results, because poorly reproduced stronger blend lines determine the global line broadening and shift of the best fit, and therefore indirectly dictate an ill-defined solution for ^{6}Li/^{7}Li. This is especially true for the case of high metallicity ([Fe/H] = +0.5) and low lithium abundance (A(Li) = 1.5), where the ^{6}Li/^{7}Li corrections obtained with line list G09 are essentially useless.

It is therefore hardly surprising that line lists G09 and M12 produce somewhat different fitting results (compare Figs. 2 and A.4), which moreover depend strongly on the wavelength range selected for fitting the Li I 670.8 nm spectral region, as well as on whether the continuum placement is a free or a fixed parameter.

The above-mentioned difficulties do not exist if we derive the 3D NLTE corrections using the line list K95 which includes only the Li I components. We also notice that the results obtained with this line list are much less sensitive to the value of $v \sin i$ than in the case of line lists G09 and M12. We argue that the fitting results obtained by considering only Li I lines must be very similar to those one would derive if all blend lines were fitted individually in the line lists G09, M12, or any other line list representative of the Li region. This argument is illustrated and supported by the investigations presented in Appendices B

and C, where we show that a line list adjusted to fit a given spectrum in 1D generally produces a less satisfactory fit when used for 3D modeling. An equally good fit in 3D can only be achieved by readjusting the line list to account for 3D abundance corrections and differential wavelength shifts of the blends. When using the 1D and 3D fine-tuned line lists, respectively, the differential 1D-3D lithium isotopic abundances become largely independent of the blend lines and are well approximated by the corrections obtained with line list K95 (only Li I).

2.5. Analytical expressions

We derived analytical expressions for the corrections derived from the "only Li" line list K95 to be able to numerically evaluate $\Delta A_{\rm 3DNLTE-1DLTE}$ and $\Delta q_{\rm 3DNLTE-1DLTE}$ as a function of the stellar parameters for any target star within the range of our grid.

As mentioned above, the A(Li) abundance corrections for all the models in our grid show only a weak dependency on the surface gravity. Assuming a $\log g$ of 4.0 or 4.5, the resulting A(Li) corrections are very similar, as shown in the lower panels of Fig. 2. Within the modeling uncertainties (see below), the $\log g$ dependence may be neglected. For this reason, we assumed $\Delta A_{\rm 3DNLTE-1DLTE}$ to be independent of $\log g$ while deriving the analytic approximation.

Somewhat unexpectedly, model atmosphere $N2$, with $T_{\rm eff} = 5920$ K, $\log g = 4.5$, [Fe/H] $= -1$, results in a smaller ΔA(Li) than expected from the trends of the corrections derived using other models in our grid (see Figs. A.1–A.3). A possible explanation for this discrepancy is that this model was computed for a smaller number of snapshots (8) in comparison to the other models (20). We decided not to use this result and instead consider it to be equal to the correction computed for the model $N1$ (with the same $T_{\rm eff}$ but $\log g = 4.0$) in deriving the numerical fitting function for $\Delta A_{\rm 3DNLTE-1DLTE}$.

We provide a link to a web page[2] that uses the analytical expressions developed in this work and allows the user to compute the $\Delta q_{\rm 3DNLTE-1DLTE}$ corrections as a function of $T_{\rm eff}$, [Fe/H], $\log g$, $v \sin i$, A(Li) and ^{6}Li/^{7}Li, and the $\Delta A_{\rm 3DNLTE-1DLTE}$ corrections as a function of $T_{\rm eff}$, [Fe/H] and A(Li). However, below we also provide simplified analytical expressions for a quick evaluation of the 3D NLTE corrections.

The simplified expressions for $\Delta A_{\rm 3DNLTE-1DLTE}$ and $\Delta q_{\rm 3DNLTE-1DLTE}$ provided in this section are based on all available data points for $v \sin i = 2.0$ km s^{-1}, A(Li) $= 2.0$, q(Li) $= 5\%$, and are functions of $T_{\rm eff}$, ($\log g$), and [Fe/H]. The two fitting functions are described by the following equations:

$$\Delta A_{\rm 3DNLTE-1DLTE} = C_0 + C_1 x + C_2 x^2 + C_3 z + C_4 z^2 + C_5 xz, \quad (1)$$

$$\Delta q_{\rm 3DNLTE-1DLTE} = \sum_{i=0}^{2} \sum_{j=0}^{1} \sum_{k=0}^{2} c_{ijk} x^i y^j z^k, \quad (2)$$

where $x \equiv (T_{\rm eff} - T^*_{\rm eff})/T^*_{\rm eff}$, $y \equiv \log g - \log g^*$, and $z \equiv$ [Fe/H], with $T^*_{\rm eff} = 5900$ K and $\log g^* = 4.0$. The valid parameter ranges are $0 \le x \le 0.1$; $0 \le y \le 0.5$; $-1.0 \le z \le +0.5$. The formulae consist of six (C_{0-5}) and 18 (c_{ijk}) numerical coefficients for ΔA and Δq, respectively (explicitly given in Table 2).

To visualize the resulting 3D NLTE corrections generated with this tool, we present in Fig. 3 the contours of $\Delta A_{\rm 3DNLTE-1DLTE}$ in the $T_{\rm eff}$ – [Fe/H] plane (upper panel), and contour plots of $\Delta q_{\rm 3DNLTE-1DLTE}$ in the $T_{\rm eff}$ – [Fe/H] and $T_{\rm eff}$ – $\log g$ plane (middle and lower panel, respectively).

[2] https://pages.aip.de/li67nlte3d

Table 2. Numerical coefficients in Eqs. (1) and (2) derived for the line list K95 with representative 1D LTE values of A(Li) $= 2.0$, q(Li) $= 5\%$, and $v \sin i = 2.0$ km s^{-1}.

Coeff.	Value	Coeff.	Value
C_0	0.074205	c_{000}	−1.5994
C_1	−0.607931	c_{010}	1.0167
C_2	1.518850	c_{001}	−0.4877
C_3	0.053601	c_{011}	0.2553
C_4	0.023510	c_{002}	−0.1548
C_5	−0.159625	c_{012}	0.3447
		c_{100}	−7.7112
		c_{110}	6.0203
		c_{101}	4.6808
		c_{111}	1.0406
		c_{102}	6.0582
		c_{112}	−12.9981
		c_{200}	−96.3931
		c_{210}	191.2326
		c_{201}	−142.0070
		c_{211}	223.2101
		c_{202}	−68.1011
		c_{212}	223.1616

The functional forms provided in this work allow a quick estimate of 3D NLTE corrections for a limited range of stellar parameters. For a complete overview and more precise 3D NLTE corrections, we refer to the table available at the CDS, and to the above-mentioned web page[2]. To give an example, our full analytical expressions give the following corrections for HD 82943 ($T_{\rm eff} = 6025$ K, $\log g = 4.53$, [Fe/H] $= +0.30$; Israelian et al. 2003): $\Delta A_{\rm 3DNLTE-1DLTE} = +0.08$ dex and $\Delta q_{\rm 3DNLTE-1DLTE} = -1.7\%$ points.

The root mean square (rms) difference between the global fitting function used by the above-mentioned web page and the input data points of the regular grid is 0.007 dex for $\Delta A_{\rm 3DNLTE-1DLTE}$ and 0.07% points for $\Delta q_{\rm 3DNLTE-1DLTE}$. These numbers represent the mean fitting function errors of the two quantities for stellar parameters that lie close to our grid points.

In order to evaluate the interpolation errors of our analytical expressions outside of the grid points, we computed $\Delta A_{\rm 3DNLTE-1DLTE}$ and $\Delta q_{\rm 3DNLTE-1DLTE}$ for intermediate $T_{\rm eff}$, $\log g$ and A(Li) values by using two additional 3D model atmospheres with [Fe/H] $= 0.0$, $\log g = 4.3$ and $T_{\rm eff} = 6110$ and 6430 K. The 3D NLTE spectra have been computed for $A({\rm Li})_{\rm 3DNLTE} = 1.5$, 1.75, 2.0, 2.25, 2.5 and for the same ^{6}Li/^{7}Li and $v \sin i$ values as in case of the original grid. The rms difference between the global fitting function and these new intermediate data points is again 0.007 dex for $\Delta A_{\rm 3DNLTE-1DLTE}$ and 0.10% points for $\Delta q_{\rm 3DNLTE-1DLTE}$. Even if we do not have the possibility to compute 3D NLTE corrections for intermediate points in [Fe/H], due to the lack of 3D hydrodynamical model atmospheres, we assume that the mean interpolation errors of 0.01 dex for ΔA and 0.10% points for Δq are valid for the whole parameter space covered by our grid. The largest errors in ΔA of ±0.015 dex are encountered at low temperatures ($T_{\rm eff} \approx 5900$ K), while the largest errors in Δq of ±0.2% points are mainly incurred at high temperatures ($T_{\rm eff} \approx 6500$ K).

2.6. 1D NLTE corrections and comparison with other works

In order to distinguish between the contributions of 3D and NLTE effects in the combined 3D NLTE correction, we repeated

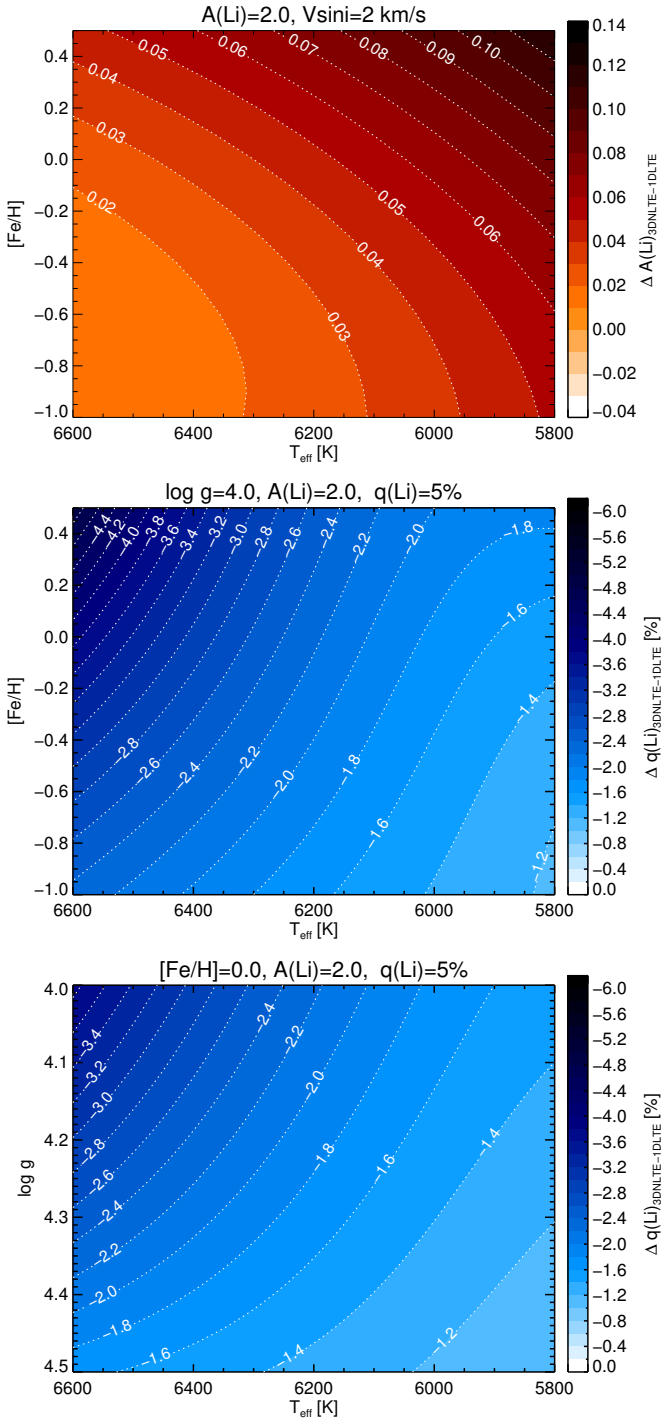

Fig. 3. Contour plots of 3D NLTE A(Li) corrections $\Delta A_{\rm 3DNLTE-1DLTE}$ (*upper panel*) and ^{6}Li/^{7}Li corrections $\Delta q_{\rm 3DNLTE-1DLTE}$ (*middle panel*) in the $T_{\rm eff}$ – [Fe/H] plane. The same 3D NLTE ^{6}Li/^{7}Li corrections in the $T_{\rm eff}$ – log g plane are shown in the *bottom panel*. The contours are computed for [Fe/H] = 0, $v \sin i = 2$ km s^{-1}, A(Li) = 2.0, and q(Li) = 5%, employing the analytical expressions in Eqs. (1) and (2) with the coefficients given in Table 2.

the same procedure for deriving the 3D NLTE corrections but replacing the grid of 3D NLTE spectra for $A(\mathrm{Li})_{\rm 3DNLTE} = 2.0$ and $q(\mathrm{Li})_{\rm 3DNLTE} = 5\%$ with an identical grid of 1D NLTE spectra. A rotational broadening of $v \sin i = 2.0$ km s^{-1} was applied to both 1D NLTE and 1D LTE spectra. The 1D NLTE corrections for ^{6}Li/^{7}Li are very close to zero, having a mean value of −0.10% with a standard deviation of 0.08%. This is expected as both LTE and NLTE line profiles are intrinsically symmetric. On the other hand, the 1D NLTE corrections for A(Li) show a similar trend as the 3D NLTE corrections, although with an offset to slightly smaller values (see Fig. 4). We have derived an equation similar to the Eq. (1) for the 1D NLTE case to facilitate the comparison with our 3D corrections and with the results from the literature (see below).

Figure 4 shows the functions for estimating the 3D NLTE and 1D NLTE A(Li) corrections derived in this work for metallicities [Fe/H] = −1.0, −0.5, 0.0, and +0.5, together with the results obtained by Takeda & Kawanomoto (2005) and Lind et al. (2009). Our 3D and 1D NLTE corrections follow similar trends but with small offset towards lower values (ranging between 0.01 and 0.03 dex, depending on [Fe/H] and $T_{\rm eff}$). This only small difference indicates that the 3D effects slightly enhance the non-LTE effects, while the latter generally dominate over the 3D effects in the combined 3D NLTE corrections.

The overall trends of our 1D NLTE corrections are similar to the trends obtained by Lind et al. (2009), with an offset ranging between 0.02 and 0.06 dex, depending mainly on the metallicity, while the curves of Takeda & Kawanomoto (2005) have a slightly different slope. Such differences in the 1D NLTE lithium abundance corrections, being ∼0.06 dex at most, are not unexpected due to the differences in the methods (model atmospheres, model atom, numerical procedure for computing departure coefficients, etc.) used by different authors. Nevertheless, we performed a test to check if the difference in the 1D NLTE A(Li) corrections could be explained by the different model atmospheres used in the spectral synthesis in this work (1D LHD models) and in Lind et al. (2009; MARCS models), respectively. The test was performed using a 1D NLTE spectrum computed from a MARCS model with $T_{\rm eff} = 6500$ K, [Fe/H] = −1, log g = 4.0, assuming $A(\mathrm{Li})_{\rm 1DNLTE} = 2.0$ and $^6\mathrm{Li}/^7\mathrm{Li}_{\rm 1DNLTE} = 5\,\%$, and a corresponding grid of 1D LTE spectra computed for combinations of nine A(Li) and nine ^{6}Li/^{7}Li values, using the same MARCS model atmospheres (Gustafsson et al. 2008) as in Lind et al. (2009). The MARCS NLTE spectrum was fitted by the grid of MARCS LTE line profiles following the same fitting procedure as described in Sect. 2.3. The resulting 1D LTE A(Li) correction is −0.055 dex, in very good agreement with the correction of −0.053 dex obtained for those stellar parameters by Lind et al. (2009). This result confirms that the shift of ∼0.05 dex between our 1D NLTE lithium abundance corrections and the ones by Lind et al. (2009; see Fig. 4, top left panel) are likely due to the different model atmospheres adopted in the spectral synthesis.

The analytical expressions given in Sbordone et al. (2010) for A(Li) were derived using 3D model atmospheres with metallicities −2 and −3 that do not overlap with our grid. Since we do not observe a linear dependence of the A(Li) 3D NLTE corrections on the metallicity, the extrapolated corrections from Sbordone et al. (2010) would be too uncertain for a useful comparison with our results. Therefore, we do not present such a comparison.

We compared the 3D NLTE corrections for ^{6}Li/^{7}Li derived in this work with the corrections presented by Steffen et al. (2012) and found very good agreement. This was expected, since the model atmospheres and methods used in these two works are similar. The present study extends the work of Steffen et al. (2012), using a 3D NLTE grid with more metallicity points around the solar value, and also investigating the dependence of the 3D NLTE corrections on A(Li), ^{6}Li/^{7}Li, $v \sin i$, and the list of blend lines.

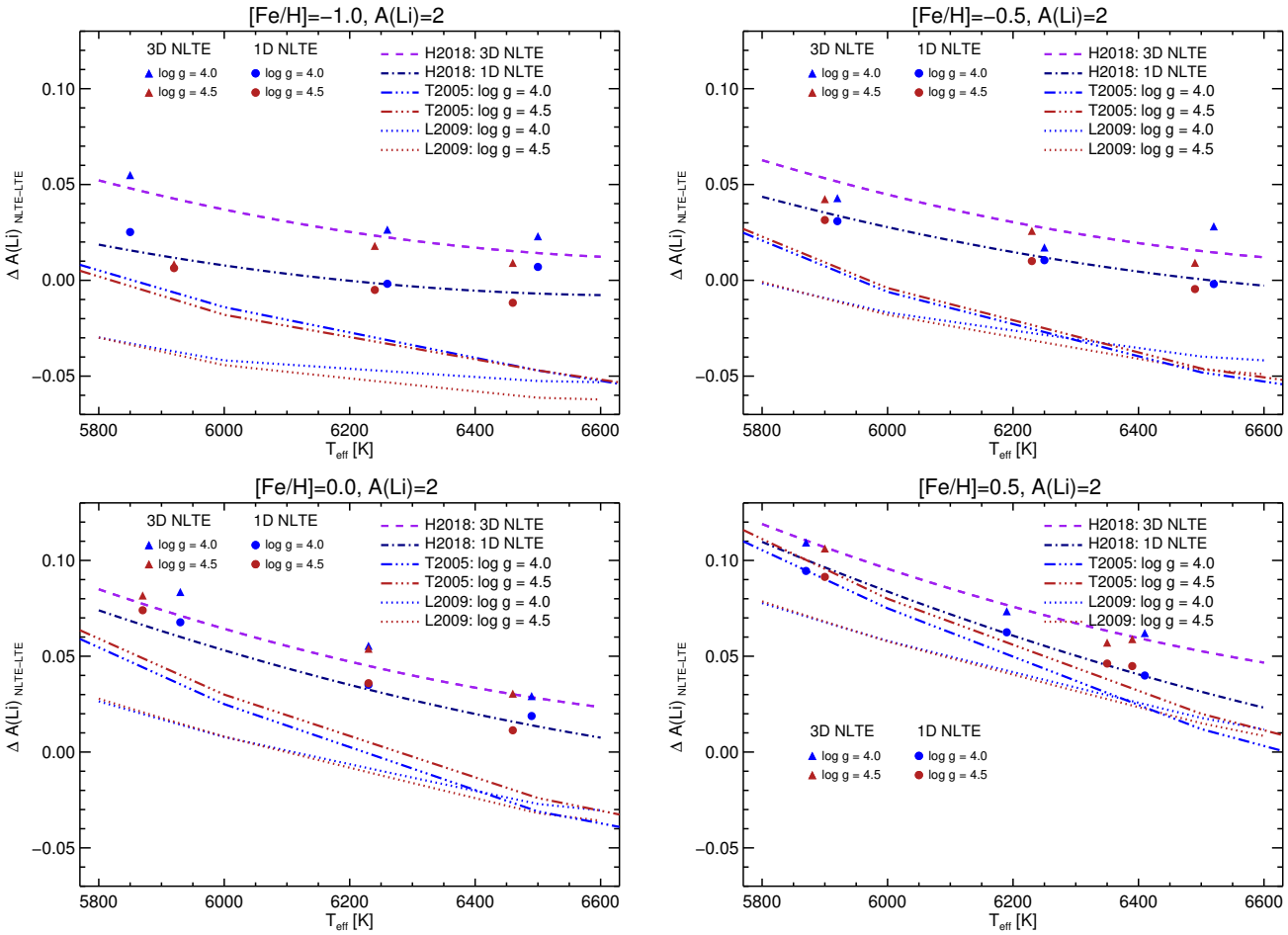

Fig. 4. Comparison of the 1D and 3D NLTE abundance corrections derived in this work with the 1D NLTE corrections from Lind et al. (2009; L2009, dotted lines) and Takeda & Kawanomoto (2005; T2005, dash-dotted lines) for metallicities −1.0, −0.5, 0.0, and +0.5 (*from top left to bottom right*). Red and blue triangles denote the individual 3D NLTE corrections, while red and blue circles denote the individual 1D NLTE corrections for A(Li) computed in this work (H2018) for log g of 4.0 and 4.5, respectively.

3. Li abundance and ^{6}Li/^{7}Li isotopic ratio in HD 207129 and HD 95456

In this section, we analyze two solar-type stars, HD 207129 and HD 95456, in order to determine A(Li) and the ^{6}Li/^{7}Li isotopic ratios, at first with a 1D LTE approach, and afterwards applying our already pre-computed 3D NLTE corrections. These stars have been selected for this study because the difference in their effective temperatures places them at two extreme positions in our correction grid. They are part of a larger sample of stars with high lithium content and low activity levels, for which high-resolution and very-high-S/N spectra are available that allow a sensitive analysis of ^{6}Li/^{7}Li. We point out that Gomes da Silva et al. (2014) performed long-term activity studies of HD 207129 and HD 95456 using Ca II H & K and Hα lines in their HARPS spectra (Mayor et al. 2003), and found both stars to show very low activity levels with no significant long-term variability.

3.1. Observations and stellar parameters

The observed spectra used in this work have been obtained with the HARPS spectrograph at La Silla observatory (ESO, Chile) within the framework of the HARPS GTO planet search program (subsample HARPS-I, Mayor et al. 2003). The spectral resolution of $R \sim 115\,000$ and the high S/N of ∼2000 of the combined spectrum of each star provide the quality that is needed for analysis of the Li I λ670.8 nm region in the context of the ^{6}Li/^{7}Li measurements.

The stellar atmospheric parameters ($T_{\rm eff}$, log g, [Fe/H] and $V_{\rm micro}$) of both stars were derived by Sousa et al. (2008) and are summarized in Table 3. The abundances of several elements with blending lines present in the line lists (Si, Ca, Ti, V) were adopted from Adibekyan et al. (2012), whereas the carbon and oxygen abundances were taken from Suárez-Andrés et al. (2017) and Bertran de Lis et al. (2015), respectively, and the nitrogen abundance was chosen to be equal to the carbon abundance. The elemental abundances adopted for the Sun, HD 207129, and HD 95456 are given in Table 4.

3.2. Rotational broadening and iron abundance

A list of atomic line data has been constructed for a number of isolated, unblended Fe I lines taken from Doyle et al. (2014), Tsantaki et al. (2013) and from the VALD-v3 database (Kupka et al. 2011) to estimate the projected rotational velocity ($v \sin i$) and the possible small iron abundance correction for the stars studied in this work. For each line of each star, a grid of nine 1D LTE Kurucz Atlas spectra was computed assuming an iron abundance range of ±0.2 dex around the adopted iron abundance (metallicity) value, with a step of 0.05 dex. The spectra

Table 3. Stellar parameters of HD 207129 and HD 95456.

Parameter	HD 207129	HD 95456
$T_{\rm eff}$ (K)	5937 ± 13	6276 ± 22
log g	4.49 ± 0.02	4.35 ± 0.04
[Fe/H]	0.00 ± 0.01	0.16 ± 0.02
$V_{\rm micro}$ (km s^{-1})	1.40 ± 0.01	1.40 ± 0.02
$v \sin i$ (km s^{-1})	2.21 ± 0.24	3.28
Δ[Fe/H]	−0.025 ± 0.063	−0.068 ± 0.067

Notes. $T_{\rm eff}$, log g, [Fe/H], $V_{\rm micro}$ and their errors are adopted from Sousa et al. (2008), and the $v \sin i$ for HD 95456 is taken from Delgado Mena et al. (2015). Δ[Fe/H] is the small iron abundance correction derived in Sect. 3.2 relative to the adopted metallicity (third row).

Table 4. Chemical abundances A(X) used in this work.

Element	Sun	HD 207129	HD 95456
C	8.50	8.44	8.67
O	8.76	8.69	8.93
Si	7.51	7.55	7.70
Ca	6.34	6.39	6.54
Ti	4.95	5.04	5.16
V	3.93	4.03	4.17
Fe	7.52	7.495	7.612

Notes. The abundances of C, O and Fe for the Sun are adopted from Caffau et al. (2011) and of Si, Ca, Ti and V from Asplund et al. (2009). For HD 207129 and HD 95456, the abundances of C and O are taken from Suárez-Andrés et al. (2017) and Bertran de Lis et al. (2015), respectively, and the abundances of Si, Ca, Ti and V are from Adibekyan et al. (2012). The Fe abundance is computed in this work (Sect. 3.2).

were computed using the 2014 version of the spectral synthesis code MOOG (Sneden 1973).

The fitting procedure was performed for the solar flux atlas from Kurucz (2005), and for the HARPS spectra of HD 207129 and HD 95456. The HARPS spectra have been locally normalized for each Fe line. We investigated the quality of the fits by eye and by means of a $\chi^2_{\rm red}$ analysis. All the lines that seemed to be blended with other spectral features (at least in one of the two stars or the Sun), or which provided a non-satisfactory fit to the observations, were excluded from the sample. Eventually, we were left with 10 "clean" Fe I lines which are well isolated and can be fitted well in the solar spectrum and the HARPS spectra of the two stars. Table 5 lists the atomic data of the selected Fe I lines: wavelength, excitation potential (EP), oscillator strength (log gf), and the reference to the source they were taken from for each individual Fe I line.

Four parameters were varied to achieve the best fit: [Fe/H], $v \sin i$, the global wavelength shift (Δv), and the continuum level. Since it was difficult to obtain both $V_{\rm macro}$ and $v \sin i$ individually from the fitting procedure due to a "degeneracy" of the solution, a fixed Gaussian macroturbulence velocity ($V_{\rm macro}$) was assumed for the fitting. $V_{\rm macro}$ was adopted from Doyle et al. (2014) and used after the application of a factor to convert the radial-tangential (RT) macroturbulence parameter ($V_{\rm RT}$) provided by these authors to the Gaussian macroturbulence parameter $V_{\rm macro}$ that we use. This conversion factor was determined for the solar case using the same solar $v \sin i$ and atmospheric parameters (including $V_{\rm micro} = 1.0$ km s^{-1}) as assumed in Doyle et al. (2014). We derive a solar [Fe/H] = −0.02 ± 0.06 and $V_{\rm macro} = 2.12 \pm 0.10$ km s^{-1} resulting in the conversion formula $V_{\rm macro} \sim 0.66\, V_{\rm RT}$. The relation between the different macroturbulence velocity models has been discussed in a recent work by Takeda & UeNo (2017), and the conversion factor of 0.66 that we derive is in agreement with their results. For a given $V_{\rm macro}$, each line profile has been broadened by nine different $v \sin i$ values with the flux convolution approximation, assuming a limb darkening coefficient of $\epsilon = 0.6$ (Gray 2005). The least-squares fitting method that we apply (MPFIT; Markwardt 2009) relies on interpolation in the grid of the precomputed synthetic spectra with different [Fe/H] and $v \sin i$. For each star, the best fit values of [Fe/H] and $v \sin i$ were averaged over the ten different Fe I lines and the uncertainties were derived from the standard deviations (cf. Table 5).

For HD 207129, we obtain $v \sin i = 2.21 \pm 0.24$ km s^{-1} and an iron abundance correction of Δ[Fe/H] = −0.025 ± 0.063 dex. For HD 95456, the radial-tangential macroturbulence is $V_{\rm RT} = 5.05$ km s^{-1} according to Doyle et al. (2014), which is large enough to broaden the synthetic line profiles to such an extent that the fits were not very different for $v \sin i$ between 0 and 3 km s^{-1}. For instance, when we use the $V_{\rm macro}$ value from Doyle et al. (2014), we obtain a formal $v \sin i$ of 0.88 km s^{-1}. As we discuss in Sect. 3.5, the measured A(Li) and ^{6}Li/^{7}Li for HD 95456 essentially do not change with different $v \sin i$ assumptions. We therefore prefer the $v \sin i$ value of 3.28 km s^{-1} determined by Delgado Mena et al. (2015), based on a combination of Fourier transform and goodness-of-fit methods. We derive a small Fe abundance correction of Δ[Fe/H] = −0.068 ± 0.067 dex (relative to the literature value of [Fe/H]) for HD 95456.

3.3. Blend lines in the lithium λ670.8 nm region

One of the challenges in ^{6}Li/^{7}Li measurements is the presence of several other atomic and molecular lines overlapping with the resonance doublet. While the contribution of these blends may be very small in metal poor stars, they become more significant at higher metallicities and must be treated carefully for stars having metallicities close to solar or higher. There are several lists of atomic and molecular lines currently available in the literature which have been carefully constructed to reproduce the Li λ670.8 nm region (e.g., Mandell et al. 2004, Ghezzi et al. 2009, Meléndez et al. 2012, Israelian 2014; priv. comm.) and are fitted for very sensitive measurements of the ^{6}Li/^{7}Li isotopic ratio in solar-type stars. It has already been demonstrated that the use of different lists of atomic and molecular lines interfering with the Li I λ670.8 nm doublet can lead to noticeable differences in the measured values of ^{6}Li/^{7}Li (e.g., Israelian et al. 2003; Mott et al. 2017). We therefore perform our analysis using different line lists provided in the literature and compare the results.

Specifically, we used three different line lists for the analysis of A(Li) and ^{6}Li/^{7}Li in the atmospheres of HD 207129 and HD 95456. In addition to G09 and M12, we used the line lists constructed by Israelian (2014; priv. comm.), as given by Mott et al. (2017; hereafter, I14). The line lists were adjusted by computing 1D LTE synthetic spectra and fitting the 670.8 nm region in the solar spectrum (G09) or in spectra of other stars (I14). The above authors assumed different elemental abundances from what we assume for the Sun (Table 4, Col. 2). Specifically, we adopted the solar abundance values for 12 elements (Li, C, N, O, P, S, K, Fe, Eu, Hf, Os, Th) from Caffau et al. (2011; their Table 5), and for other elements we used the internal solar elemental abundances

Table 5. Fe I lines used for deriving $v \sin i$ and the iron abundance correction Δ[Fe/H].

Spectral line parameters					Sun		HD 207129		HD 95456	
Chemical Species	Wavelength λ (Å)	EP (eV)	log gf (dex)	Source	$V_{\rm macro}$ (km s^{-1})	Δ[Fe/H] (dex)	$v \sin i$ (km s^{-1})	Δ[Fe/H] (dex)	$v \sin i$ (km s^{-1})	Δ[Fe/H] (dex)
Fe I	6094.3800	4.650	−1.566	T13	2.14	−0.088	2.53	−0.088	1.58	−0.118
Fe I	6200.3190	2.609	−2.437	Do14	2.06	−0.019	1.97	−0.022	0.00	−0.091
Fe I	6481.8800	2.280	−2.929	T13	1.94	−0.078	1.95	−0.074	0.00	−0.130
Fe I	6593.8800	2.430	−2.384	T13	2.05	−0.049	1.94	−0.055	0.00	−0.134
Fe I	6699.1408	4.593	−2.101	Vald3	2.23	−0.078	2.14	−0.119	1.59	−0.112
Fe I	6703.5655	2.759	−3.160	Vald3	2.00	0.068	2.04	0.069	0.61	0.0419
Fe I	6725.3553	4.103	−2.300	Vald3	2.23	0.051	2.41	0.052	1.12	0.0288
Fe I	6726.6658	4.607	−1.094	Vald3	2.19	0.021	2.39	0.016	1.40	−0.037
Fe I	6810.2570	4.607	−0.986	Do14	2.15	−0.044	2.24	−0.049	0.98	−0.111
Fe I	6857.2490	4.076	−2.150	Do14	2.17	0.010	2.53	0.019	1.51	−0.015
Average					2.12	−0.021	2.21	−0.025	0.88	−0.068
Std. dev.					±0.10	±0.056	±0.24	±0.063	±0.68	±0.067

Notes. The lines and their parameters are adopted from the VALD-v3 database Kupka et al. (2011; Vald3), Tsantaki et al. (2013; T13) or Doyle et al. (2014; Do14), as indicated in the fifth column. For the Sun, we used a fixed $v \sin i$ of 1.9 km s^{-1}in order to derive its $V_{\rm macro}$, whereas for HD 207129 and HD 95456 we proceeded the other way round, fixing the $V_{\rm macro}$ values at 2.33 and 3.33 km s^{-1}, respectively, in finding their $v \sin i$ (see Sect. 3.2).

of the 2014 version of MOOG, which is based on the solar abundances recommended by Asplund et al. (2009).

A molecule that is present in all line lists representing the Li I 670.8 nm region is CN. The presence of several lines of this molecule is important in the ^{6}Li determination, and assuming the correct C, N, and O abundances (because O can influence the equilibrium of the molecular reaction network) can be crucial. Particularly, the assumptions for solar abundances of O and N were significantly different between the authors of the line lists and our work. Therefore, we made some calibrations to eliminate the differences arising from different assumptions of solar abundances while constructing the line lists for performing our ^{6}Li/^{7}Li analysis. In case of O and N, our abundances were lower by up to 0.17 and 0.19 dex, respectively, and by 0.06 dex for C. In this case, we have scaled the log gf values of all the CN lines in this region by a constant factor. This factor was derived by fitting the solar flux atlas with a pre-computed grid of 1D LTE synthetic spectra for the Sun. For each line list, a grid of 1D LTE spectra was computed applying different factors (within the range of ±0.3 dex with a step of 0.01 dex) to the log gf values of all the CN lines. Then, for a given line list, we adopted the log gf factor resulting in the best fit (χ^2 minimization) to the solar flux atlas. This factor was +0.20 dex in case of the G09 and M12 line lists, and +0.19 dex in case of the I14 line list. For elements other than C, N, and O present in the line lists, the small solar abundance differences were taken into account by applying corresponding corrections to the log gf values of the individual lines of each element. After this adjustment, all line lists are "normalized" to our adopted solar abundances.

In addition, the wavelength and the log gf value of the V I line at 670.81096 nm have been updated according to the recently published values by Lawler et al. (2014). This blend is positioned close to one of the ^{6}Li components and may affect the result of the ^{6}Li/^{7}Li determination if incorrect line parameters are assumed (see Sect. 3.7).

3.4. Spectral synthesis for A(Li) and ^{6}Li/^{7}Li studies of HD 207129 and HD 95456

In order to derive A(Li) and ^{6}Li/^{7}Li in the two solar-type stars, we perform a standard 1D LTE analysis using the 2014 version of the spectral synthesis code MOOG (Sneden 1973) together with Kurucz ATLAS9 1D model atmospheres (Kurucz 1993).

A grid of 1D LTE synthetic spectra has been computed for each star. The precomputed line profiles cover a range in lithium abundance defined by the expected A(Li) (literature value, Delgado Mena et al. 2015) ±0.5 dex with a step of 0.05 dex, and a range in q(Li) between 0 and 20% with a step of 1%.

For each star, the third dimension of the grid is defined by a variation of the C, N, O abundances. These abundances were scaled together by the same factor within a range of ±0.2 dex around the fiducial C, N, O abundances and with a step of 0.05 dex, such that the grid of spectra includes nine different CNO values. The Fe I line at ~670.74 nm, being one of the strongest blends in this region, can also play an important role in the ^{6}Li/^{7}Li analysis. Therefore, we extend our grid by computing the spectra with different [Fe/H] values, which vary around the fiducial Fe abundance by ±0.1 dex, with a step of 0.1 dex for HD 207129 and 0.05 dex for HD 95456.

Thus, a four-dimensional (4D) grid of 1D LTE spectra is obtained for combinations of 21 A(Li), 21 ^{6}Li/^{7}Li, nine CNO abundances, and three (five) different [Fe/H] values, both for HD 207129 and HD 95456. In addition, these grids of spectra for both stars were replicated for three different line lists (G09, M12, I14). For the estimation of the systematic errors of A(Li) and ^{6}Li/^{7}Li due to uncertainties in effective temperature and surface gravity, the 4D grids for both stars were also computed for model atmospheres with $T_{\rm eff}$ ± 50 [K] and log g ± 0.1, but only for line list G09, and for the Fe and CNO abundance correction factors from the best fit for that line list. In total, 37485 and 61299 1D LTE synthetic spectra were computed for HD 207129 and HD 95456, respectively.

3.5. Fitting procedure for the HARPS spectra

To fit the observed spectra of the two target stars, we followed a procedure similar to the one already described in Sect. 2.3. The HARPS spectra of HD 207129 and HD 95456 were fitted through interpolation across a grid of 1D LTE line profiles computed with MOOG for line lists G09, M12 and I14.

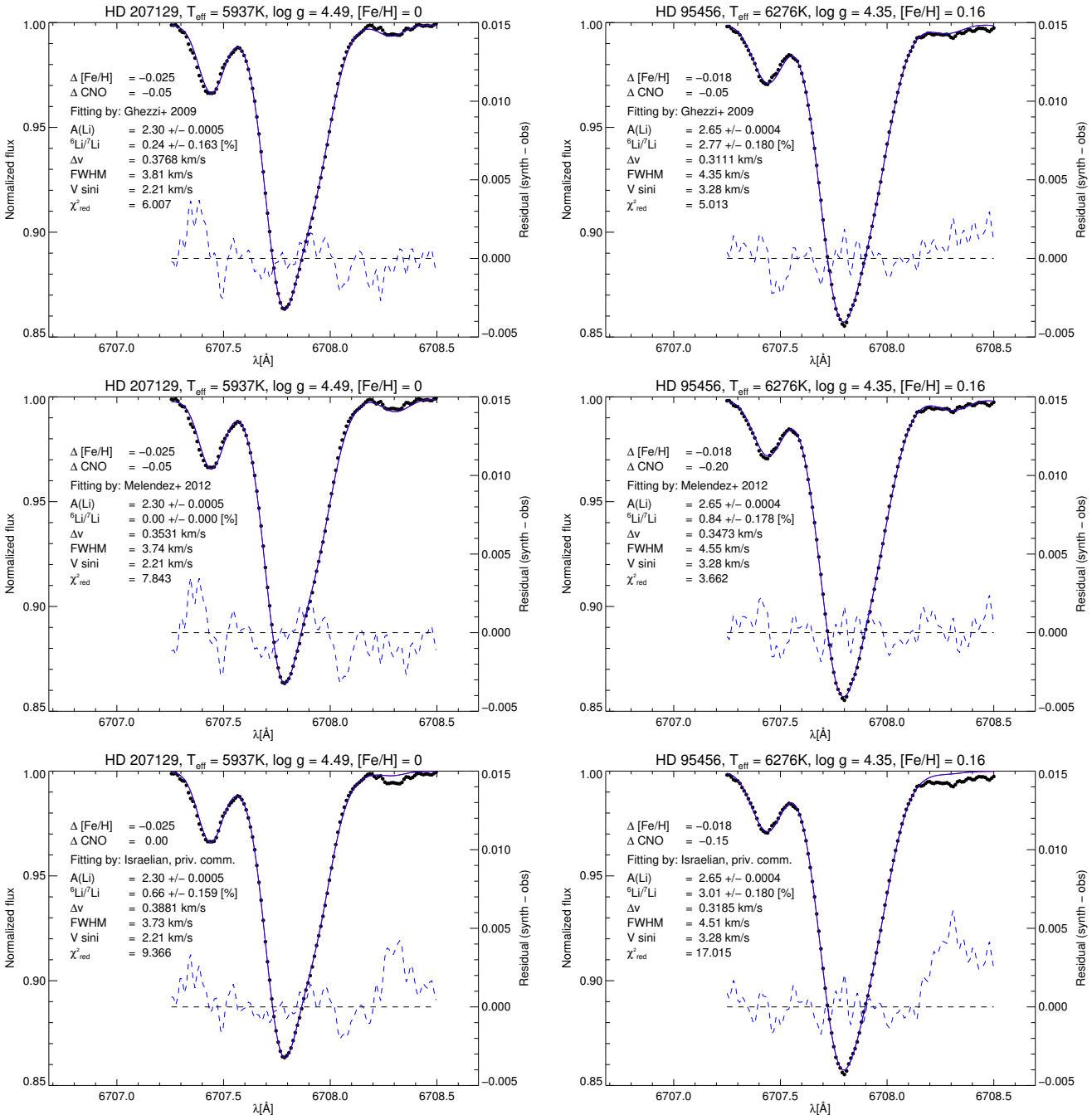

Fig. 5. The best fitting 1D LTE spectrum (solid line) superimposed on the HARPS spectrum (dots) for HD 207129 (*left panels*) and HD 95456 (*right panels*). The synthetic line profiles are computed adopting the line lists G09, M12, and I14 (*from top to bottom*), with modifications described in Sect. 3.3. The right *y*-axis defines the scale of the residuals (dashed line).

To achieve the best fit evaluated by means of a $\chi^2_{\rm red}$ minimization method, four free parameters were varied: A(Li), q(Li), the global wavelength shift (Δv) and the FWHM of the Gaussian line broadening, which accounts also for $V_{\rm macro}$, while $v \sin i$ and $V_{\rm micro}$ are fixed at the values given in Table 3. Additionally, for each combination of stellar parameters and line list, we used the 1D LTE spectra assuming different Fe, and CNO abundances. This allowed us to achieve an even better fit, allowing for possible small abundance deviations from the adopted values. We applied a similar fitting procedure to derive the lithium abundance and ^{6}Li/^{7}Li isotopic ratio in the Sun (Sect. 3.8).

3.6. Fitting results for HD 207129 and HD 95456

Figure 5 shows the best 1D LTE fit to the HD 207129 (left panels) and HD 95456 (right panels) HARPS spectra, obtained with line lists G09, M12, and I14 (from top to bottom). The best fit with line list G09 is achieved for Δ [Fe/H] = −0.025 and Δ CNO = −0.05 for HD 207129, resulting in A(Li) of 2.30 and ^{6}Li/^{7}Li of 0.2% in this star. For HD 95456, the best fit with line list G09 is obtained for Δ [Fe/H] = −0.018 and for Δ CNO = −0.05, resulting in A(Li) = 2.65 and ^{6}Li/^{7}Li = 2.8%. The Gaussian $V_{\rm macro}$ for which the best fit is achieved is 2.29 and 2.61 km s^{-1} for HD 207129 and HD 95456, respectively. For

Table 6. Best fitting results for A(Li) and ^{6}Li/^{7}Li derived for HD 207129 and HD 95456 using the line lists G09, M12 and I14 before and after the application of the 3D NLTE corrections.

		1D LTE							3D NLTE	
Star	Line list	A(Li)	^{6}Li/^{7}Li [%]	$\chi^2_{\rm red}$	Δ[Fe/H]	Δ CNO	Δ Si	Δ V	A(Li)	^{6}Li/^{7}Li [%]
HD 207129	G09	2.30	0.2	6.0	−0.025	−0.05	–	–	2.37 ± 0.04	−0.9 ± 0.68
	M12	2.30	0.0	7.8	−0.025	−0.05	–	–	2.37	−1.1
	I14	2.30	0.7	9.4	−0.025	0.00	–	–	2.37	−0.4
HD 95456	G09	2.65	2.8	5.0	−0.018	−0.05	–	–	2.70 ± 0.04	0.9 ± 1.36
	M12	2.65	0.8	3.7	−0.018	−0.20	–	–	2.70	−1.1
	I14	2.65	3.0	17.0	−0.018	−0.15	–	–	2.70	1.1
Sun (Case A)	G09	0.99	0.12	1.05	0.000	0.000	0.000	0.000	1.09 ± 0.03	−0.7 ± 2.0
Sun (Case B)	G09	0.98	1.71	1.00	−0.012	0.073	0.000	0.000	1.08 ± 0.03	0.9 ± 2.9
Sun (Case C)	G09	0.98	0.71	0.94	−0.011	0.073	0.017	−0.045	1.08 ± 0.03	−0.1 ± 4.1

Notes. For reference, we also show the fitting result for the Sun obtained with line list G09. The 3D NLTE values are obtained by applying the 3D NLTE corrections for A(Li) and ^{6}Li/^{7}Li to the 1D LTE results. Δ CNO and Δ[Fe/H] represent the additional corrections applied to CNO and Fe abundances, respectively, to obtain the best fit. For the Sun only, Δ Si and Δ V are further corrections of the silicon and vanadium abundance in the final fit. The errors of A(Li) and ^{6}Li/^{7}Li for the two stars are computed for line list G09 and include the uncertainties related to the different lists of blend lines (see Sect. 3.6). For the Sun, the error in A(Li) corresponds to a continuum placement uncertainty of ±0.05%, while the error in ^{6}Li/^{7}Li is the formal 1 σ fitting error.

HD 207129, this $V_{\rm macro}$ is in good agreement with the $V_{\rm macro}$ used for fitting the Fe I lines given in Table 5 (Sect. 3.2). For HD 95456, the $V_{\rm macro}$ derived with this procedure is lower, since we adopted a larger $v \sin i$ (Table 3) than its resulting value from the fitting of the Fe I lines (Sect. 3.2). The errors given in Fig. 5 are the 1 σ formal fitting errors. The 1D LTE best-fit values for A(Li) and ^{6}Li/^{7}Li for all three line lists are collected in Table 6. The different line lists result in somewhat different ^{6}Li/^{7}Li for the same star. We adopt the results obtained using line list G09 as the representative result of our analysis since ^{6}Li/^{7}Li obtained with this set of blends falls between the values from the analysis with line lists M12 and I14. The uncertainty due to the different line lists is included as one contribution to the total error (see below).

Figure 6 shows the best fitting $\chi^2_{\rm red}$ values obtained by fitting the HARPS spectra of HD 207129 (upper panel) and HD 95456 (lower panel) with synthetic 1D LTE spectra computed for all the combinations of Fe and CNO abundances based on the preferred line list G09. From this figure, it is clear that the lowest $\chi^2_{\rm red}$ values are obtained around the adopted abundances of Fe and CNO. We note that the best fits shown in Fig. 5 are based on the optimal choice of [Fe/H] and CNO derived from Fig. 6.

The 3D NLTE corrections for the lithium abundance and ^{6}Li/^{7}Li for HD 207129 and HD 95456 were obtained using the analytical approximations developed in this work. The 3D NLTE corrections of A(Li) were computed as a function of $T_{\rm eff}$, [Fe/H], and A(Li), the 3D NLTE corrections of ^{6}Li/^{7}Li as a function of $T_{\rm eff}$, $\log g$, [Fe/H], $v \sin i$, A(Li) and ^{6}Li/^{7}Li. We derive 3D NLTE A(Li) corrections of +0.07 dex and +0.05 dex, and ^{6}Li/^{7}Li corrections of −1.1 and −1.9% points for HD 207129 and HD 95456, respectively. Afterwards, we applied these corrections to the measured 1D LTE best-fitting values of A(Li) and ^{6}Li/^{7}Li. The derived values after such corrections are also presented in Table 6.

We compute the errors of the 1D LTE lithium abundance and ^{6}Li/^{7}Li by considering seven sources of uncertainty: uncertainties related to the choice of the effective temperature ($\triangle T_{\rm eff} = \pm 50$ [K]) and surface gravity ($\triangle \log g = \pm 0.1$) as well as the continuum placement (1.0 ± 0.05%), the internal fitting error, the fitting errors related to different Fe (Δ [Fe/H] is ±0.1 for HD 207129 and ±0.05 for HD 95456) and CNO abundance factors (Δ CNO = ±0.05). These six errors are computed for the line list G09. The seventh error is related to the different lists of atomic and molecular blends used in this work, and for both lithium abundance and isotopic ratio is computed as the standard deviation of measured A(Li) and ^{6}Li/^{7}Li, respectively, adopting line lists G09, M12, and I14. These seven different error contributions are combined in quadrature and are given as the total error in Table 6.

Finally, to test the dependence of our results on the used $v \sin i$ value, we applied a $v \sin i$ of 0.85 km s^{-1} to the synthetic spectra of HD 95456, as measured in Sect. 3.2 using Fe I lines, and repeated the fitting procedure for the best fitting values of Fe and CNO abundance for the line list G09. The resulting LTE values of A(Li) = 2.65 and q(Li) = 2.7% are in very good agreement with the values derived assuming $v \sin i = 3.28$ km s^{-1}, demonstrating that an accurate determination of the rotational broadening is not critical.

3.7. Tests with the Si I and V I lines

As mentioned in Sect. 3.3, the measurement of the ^{6}Li/^{7}Li isotopic ratio is sensitive to the list of atomic and molecular lines adopted for the spectral synthesis. In the case of HD 95456, we find a difference as high as ∼2.2%, where the lowest ^{6}Li/^{7}Li is 0.8% when the M12 line list is adopted, and the highest ^{6}Li/^{7}Li is 3.0% when I14 is used (see Table 6). The differences among the line lists arise not only from the adopted atomic data of specific lines (wavelength, $\log gf$, excitation potential), but also from the different chemical elements present in each particular list of blends.

The Si I 670.8025 nm line is of particular interest since it lies very close to the ^{6}Li feature and has been shown to have an impact on the ^{6}Li/^{7}Li measurements (e.g., Israelian et al. 2001, 2003). This line was first introduced by Müller et al. (1975) in their analysis of the solar spectrum and later investigated in detail by Israelian et al. (2003) in a number of solar-type metal-rich stars. The latter authors have shown that the Si I line at 670.8025 nm is the best candidate for this unidentified feature severely blended with the ^{6}Li line. We also note that this line has

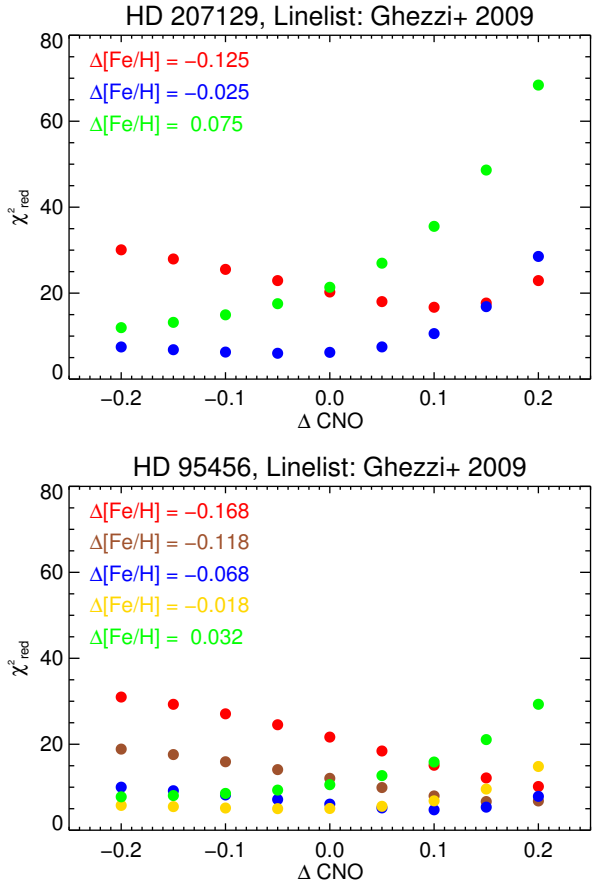

Fig. 6. The best $\chi^2_{\rm red}$ obtained by fitting the HARPS spectra of HD 207129 (*upper panel*) and HD 95456 (*lower panel*) with grids of 1D LTE line profiles computed for combinations of different Fe and CNO abundances. The line list G09 is adopted after some modifications described in Sect. 3.3. For each point, the minimum $\chi^2_{\rm red}$ is obtained by optimizing A(Li) and ^{6}Li/^{7}Li at given [Fe/H] and CNO abundance.

been assigned different parameters in the three line lists we use in this work. While the wavelength differences are rather small (670.8023 nm in G09 and M12, and 670.8025 nm in I14), the $\log gf$ values are quite different (−2.91 in G09, −2.80 in M12 and −2.97 in I14).

In a recent work by Bensby & Lind (2018), the authors noted that new laboratory measurements showed no sign of a Si I line at 670.8025 nm, referring to a private communication source (Henrik Hartmann). However, as it has been demonstrated that a "fictitious" Si I line with the assigned atomic parameters is able to reproduce the unknown blend rather well (Müller et al. 1975; Israelian et al. 2003; Mandell et al. 2004), it is still the best choice for a reliable ^{6}Li/^{7}Li analysis in solar-type stars. By no means should the new measurements be taken as justification to simply remove the "fictitious" Si I line from the list of blends, as long as the unknown feature has not been unambiguously identified.

We tested to what extent the differences in the Si I line parameters, particularly in the $\log gf$ value, can affect the ^{6}Li/^{7}Li measurement. For this purpose, we performed the same 1D LTE analysis as described in Sect. 3.5, but for different silicon abundance values at fixed Fe and CNO abundance. For each silicon abundance, the grid of lithium abundances covers 21 A(Li) times 21 ^{6}Li/^{7}Li values. This test is performed for HD 95456 only, where the derived 1D LTE ^{6}Li/^{7}Li appears to be significantly different from zero.

Figure 7 shows the $\chi^2_{\rm red}$ (upper panel) of the best fit and the resulting ^{6}Li/^{7}Li (middle panel) plotted vs. the deviation (in dex) from the adopted silicon abundance for line lists G09 (red circles), M12 (green triangles), and I14 (blue stars). It is worth noting that, when the silicon abundance is reduced, the measured ^{6}Li/^{7}Li increases, showing that changing the silicon abundance by just 0.1 dex can alter the measured ^{6}Li/^{7}Li by more than 1% point for this star, while the reduced $\chi^2_{\rm red}$ value changes only marginally. Furthermore, after increasing the Si abundance by a certain amount, depending on the line list (+0.3, +0.2, and +0.4 dex for G09, M12 and I14, respectively), the measured ^{6}Li/^{7}Li reaches 0%, indicating that the potential ^{6}Li feature is fully (over-)compensated by the Si I line.

This test shows that the atomic data of this particular blend line are very important for the measurements of ^{6}Li/^{7}Li in solar-type stars, as suggested by Israelian et al. (2003), and might be the main factor responsible for the differences in the results achieved with the different line lists. It is worth noting that the $\log gf$ of this line was calibrated by Israelian et al. (2003) in high-S/N spectra of several solar-type stars (as well as the Sun) with different effective temperatures and metallicities. In the alternative case of G09 and M12 line lists, the $\log gf$ of this line and of other blend features have been adjusted in order to better reproduce the solar spectrum.

In fact, if we assume the same $\log gf$ for the Si I line in all the line lists, the results appear to be in very good agreement despite differences in the other adopted blends. This shows that differences in $\log gf$ of the Si I line are indeed the reason for the differences in the ^{6}Li/^{7}Li isotopic ratio. We can assume that this is generally the case, at least for stars with atmospheric parameters similar to HD 95456.

Because of the recently revised $\log gf$of the V I blend, we repeat the same test as above also for the V I line. Lawler et al. (2014) gave a $\log gf$ higher by 0.3–0.5 dex, dependent on the line list considered. The resulting plot (Fig. 7, lower panel) indicates that this line does not considerably affect the ^{6}Li/^{7}Li measurement, giving differences of $\Delta q \sim 1\%$ point for a 1-dex change in the vanadium abundance. Therefore, this line is not expected to change the ^{6}Li/^{7}Li result significantly, at least for stars with stellar parameters similar to HD 95456.

3.8. Fitting results for the Sun

We applied a similar fitting procedure to derive the lithium abundance and the ^{6}Li/^{7}Li isotopic ratio in the Sun by fitting the solar flux atlas of Kurucz (2005). The 1D LTE synthetic line profiles were computed from a solar ATLAS9 model ($T_{\rm eff}$ = 5770 K, $\log g$ = 4.44, $V_{\rm micro}$ = 1.24 km s^{-1}, $\alpha_{\rm MLT}$ = 1.25; see Kurucz 1993) with MOOG for combinations of 21 A(Li) and 21 ^{6}Li/^{7}Li values, assuming a rotational broadening of $v \sin i$ = 1.9 km s^{-1}.

Using line list G09 (with modifications described in Sect. 3.3) and fixing the continuum level at c_1 = 0.9975 (relative to the continuum placement of the solar flux atlas) as in Ghezzi et al. (2009), the best fit was obtained for A(Li) = 0.99 ± 0.01 dex and ^{6}Li/^{7}Li = 0.12 ± 2.0% (Case A, Table 6), where the errors are the 1 σ formal fitting errors. The derived isotopic ratio close to zero reflects the fact that Ghezzi et al. (2009) constructed their line list under the assumption that ^{6}Li/^{7}Li = 0. An even better fit of the solar Li region can be achieved by allowing small adjustments in the continuum level and in the abundances of Fe and CNO, as described above for the stellar fits. In this case, the best fit was obtained for c_1 = 0.9977, A(Li) = 0.98 ± 0.015 dex and ^{6}Li/^{7}Li = 1.71 ± 2.9% (Case B, Table. 6). Allowing in addition slight adjustments of the Si and V

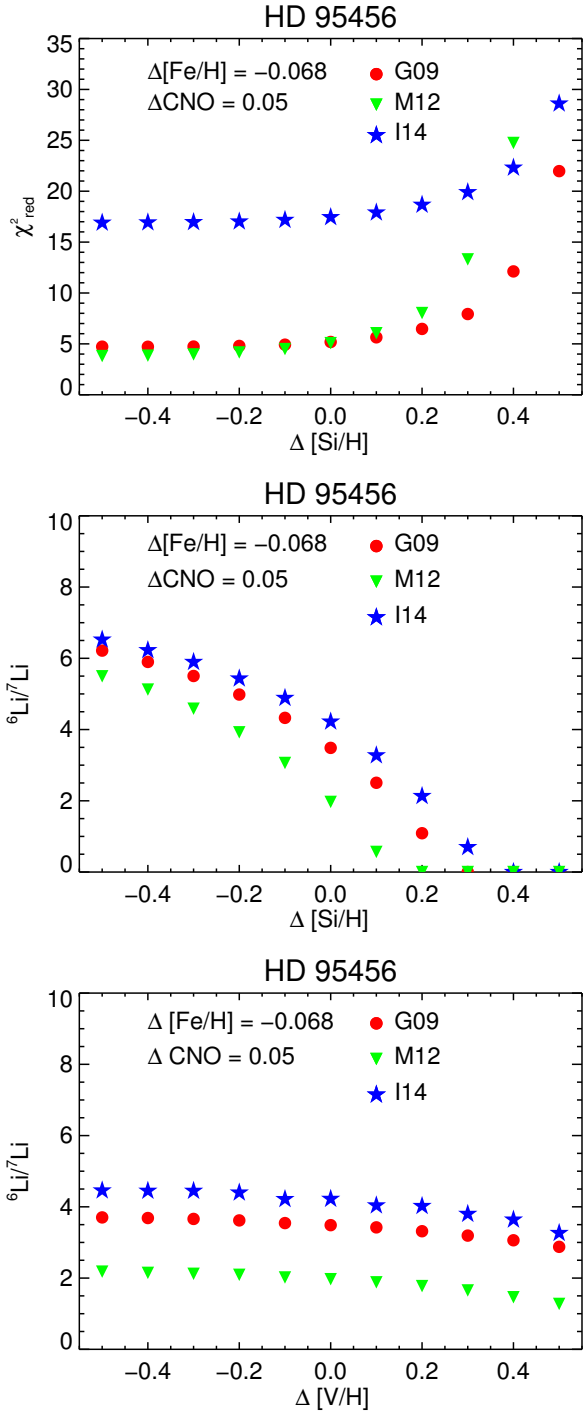

Fig. 7. The best-fitting χ^2_{red} (*upper panel*) and ^{6}Li/^{7}Li (*middle panel*) for different Si abundances, and ^{6}Li/^{7}Li for different *V* abundances (*lower panel*) for HD 95456, using line lists G09 (red circles), M12 (green triangles), and I14 (blue stars), with modifications as described in Sect. 3.3. For each point, the minimum χ^2_{red} is obtained by optimizing *A*(Li) and ^{6}Li/^{7}Li at given abundances of CNO, Fe, and Si (*upper* and *middle panels*) or V (*lower panel*).

abundances leads to a marginal improvement of the fit, but with even larger formal fitting errors: $c_1 = 0.9977$, $A(\mathrm{Li}) = 0.98 \pm 0.02$ dex, $^6\mathrm{Li}/^7\mathrm{Li} = 0.71 \pm 4.1\%$ (Case C, Fig. 8).

For the Sun, our grid of 3D NLTE corrections suggests (after slight extrapolation) $\Delta A_{\mathrm{3DNLTE-1DLTE}} \sim +0.1$ dex and $\Delta q_{\mathrm{3DNLTE-1DLTE}} \sim -0.73\%$, while the direct calculation of the corrections from 3D NLTE and 1D LHD synthetic solar Li

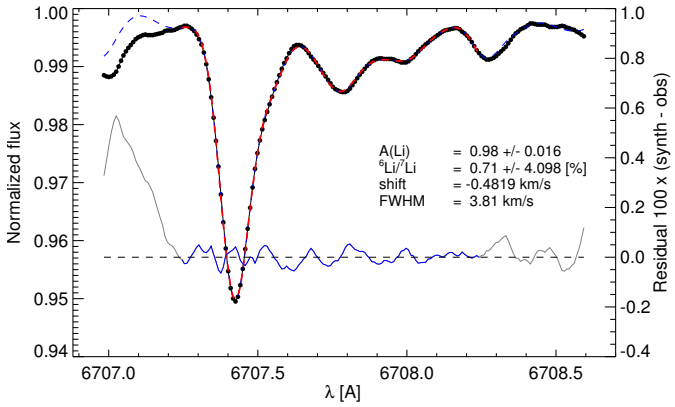

Fig. 8. The best fitting 1D LTE ATLAS/MOOG spectrum (dashed line) superimposed on the solar flux atlas spectrum of Kurucz (2005; black dots), fixing the continuum level at 0.9977 (relative to the continuum placement of the flux atlas), and using line list G09 (with modifications described in Sect. 3.3) and slight adjustments in the strengths of the CN, Fe, Si, and V lines (see Case C, Table 6) The right *y*-axis defines the scale of the residuals (thin blue line).

line profiles by the method described in Sect. 2.3 yields $\Delta A_{\mathrm{3DNLTE-1DLTE}} \sim +0.1$ dex and $\Delta q_{\mathrm{3DNLTE-1DLTE}} \sim -0.83\%$.

After applying the 3D NLTE correction for *A*(Li) to our 1D LTE best fit result (Case C), we obtain $A(\mathrm{Li}) = 1.08 \pm 0.03$, where the error is estimated from measurements with different continuum locations (best fit location ±0.05%). The ^{6}Li/^{7}Li isotopic ratio obtained from the best 1D LTE fit (Fig. 8) is −0.1% after application of the 3D NLTE correction of −0.83%, with a large formal fitting error of ±4%.

The lithium abundance obtained in this way is in very good agreement with a recent 3D NLTE analysis of a very-high-resolution PEPSI spectrum of the Li I λ 670.8 nm region of the Sun by Strassmeier et al. (2018) who measured $A(\mathrm{Li}) = 1.09 \pm 0.04$. Their estimate of $^6\mathrm{Li}/^7\mathrm{Li} = 1.4 \pm 1.6\%$ agrees with our above ^{6}Li/^{7}Li value within the large error bars.

We point out that Strassmeier et al. (2018) also employed line list G09, which is custom-made for 1D modeling and therefore leads to an inferior fit when used unaltered for 3D spectrum synthesis. This is very likely the reason why the derived ^{6}Li/^{7}Li is not fully consistent with our corrected 1D result, $^6\mathrm{Li}/^7\mathrm{Li} \approx 0$. A more consistent fit in 3D can only be achieved if the line list is adapted to account for 3D effects, in particular adjusting the strength and wavelength of the silicon line (see Appendix B). We present a detailed comparison of fine-tuned 3D and 1D fits to the solar Li I λ 670.8 nm spectral region in Appendix C.

4. Summary and conclusions

We presented 3D NLTE corrections for lithium abundance, *A*(Li), and the ^{6}Li/^{7}Li isotopic ratio, *q*(Li), based on a six-dimensional grid of 3D NLTE spectra. The stellar parameters defining the grid are effective temperatures, T_{eff} (3 different values), gravity, $\log g$ (2), microturbulence velocity, V_{micro} (3), metallicity, [Fe/H] (4), lithium abundance, $A(\mathrm{Li})_{\mathrm{3DNLTE}}$ (3), and isotopic ratio, $q(\mathrm{Li})_{\mathrm{3DNLTE}}$ (3; see Sect. 2 for details). In addition, four different $v \sin i$ values of rotational broadening were applied to the 3D NLTE and 1D LTE spectra. For each list of atomic and molecular blend lines (K95, G09, and M12), this results in a total of 2592 3D NLTE corrections for both *A*(Li) and *q*(Li). The results obtained using the line lists G09 and M12 depend strongly on the wavelength range selected for fitting the Li I

670.8 nm spectral region, as well as on whether the continuum placement is a free or a fixed parameter. As a consequence, the 3D NLTE ^{6}Li/^{7}Li corrections depend on the atomic and molecular blends used for the spectral line synthesis. Eventually, we rely only on the 3D NLTE corrections based on line list K95 (Li only). This definition is supported by detailed fits of the solar Li spectral region with both 1D- and 3D-based synthetic spectra computed with fine-tuned line lists (Appendix C).

^{6}Li/^{7}Li derived by fitting a given 3D NLTE spectrum with the grid of 1D LTE line profiles is found to be always larger than the input 3D NLTE values by 0.4–4.9% for the range of stellar parameters studied in this work. This implies that a 1D LTE spectral analysis leads to an overestimation of the ^{6}Li/^{7}Li isotopic ratio by up to 4.9% points in solar-type stars covered by our grid. The 3D NLTE corrections, $\Delta q_{\rm 3DNLTE-1DLTE}$, are therefore always negative.

The corrections show a systematic dependence on the stellar parameters. For a given metallicity, generally $\Delta q_{\rm 3DNLTE-1DLTE}$ becomes larger with higher $T_{\rm eff}$ and lower $\log g$. For given $T_{\rm eff}$ and $\log g$, they become larger with higher metallicity, A(Li), and isotopic ratio q(Li). Moreover, we observe a dependence of $\Delta q_{\rm 3DNLTE-1DLTE}$ on the applied rotational broadening: the higher the $v \sin i$, the smaller the corrections. Furthermore, the quality of the fit improves assuming higher $v \sin i$ values applied simultaneously to the 3D NLTE and 1D LTE spectra, leading to lower values of $\chi^2_{\rm red}$ (but also implying larger fitting errors). On the other hand, we observe only a very weak variation of $\Delta q_{\rm 3DNLTE-1DLTE}$ with the small changes (± 0.5 km s^{-1}) of the microturbulence parameter, and therefore adopt the results obtained assuming the central $V_{\rm micro}$ values as representative corrections.

Similarly, the abundance corrections, $\Delta A_{\rm 3DNLTE-1DLTE}$, show a systematic dependence on the stellar parameters. For a given [Fe/H], they generally become larger towards lower $T_{\rm eff}$. We observe small variations of $\Delta A_{\rm 3DNLTE-1DLTE}$ for different $\log g$ values (4.0 or 4.5) and A(Li), whereas the dependence on ^{6}Li/^{7}Li, $V_{\rm micro}$, and $v \sin i$ is negligible. The 3D NLTE correction for A(Li) turned out to be very similar for different lists of the atomic and molecular data used for the spectral line synthesis. They are found to range between -0.01 and $+0.11$ dex.

We provide analytical expressions (Eqs. (1) and (2)) which allow to estimate the 3D NLTE correction for A(Li) and ^{6}Li/^{7}Li as a function of $T_{\rm eff}$, $\log g$, and [Fe/H] (see Sect. 2.5). These mathematical functions are valid for the representative values A(Li) = 2.0, q(Li) = 5%, and $v \sin i = 2$ km s^{-1} for a quick evaluation of the 3D NLTE corrections in the investigated range of stellar parameters. For full details, we provide a (electronic) table with the complete grid of the 3D NLTE corrections, and a link to a web page that allows the user to compute the 3D NLTE corrections of A(Li) as a function of $T_{\rm eff}$ [Fe/H], and A(Li), and the 3D NLTE corrections of ^{6}Li/^{7}Li as a function of $T_{\rm eff}$, $\log g$, [Fe/H], $v \sin i$, A(Li) and ^{6}Li/^{7}Li.

Our analytical expressions, valid for solar-type stars, allow to account for 3D plus NLTE effects without the need of direct access to complex 3D NLTE computations. This is particularly important when a large sample of stars needs to be analyzed in terms of lithium abundance and isotopic ratio, since 3D NLTE analysis for even a single target is computationally demanding and time consuming. The analysis of the observed spectra can be carried out at first by using standard 1D LTE spectrum synthesis techniques. Afterwards, the 1D results can be corrected for the 3D NLTE effects by applying the precomputed 3D NLTE corrections interpolated to the desired set of stellar parameters.

In the second part of this work, we use high-quality HARPS spectra of two solar-type stars in order to derive the A(Li) and ^{6}Li/^{7}Li in their atmospheres. The stars were selected because they are located at opposite sides of the investigated $T_{\rm eff}$ range where the corrections show the largest differences. The lithium doublet in these two stars was first analyzed with a standard 1D LTE approach, and subsequently corrected for 3D NLTE effects using the pre-computed 3D NLTE corrections. After applying the 3D NLTE corrections, we obtain A(Li) = 2.37 ± 0.04 and ^{6}Li/^{7}Li = −0.9% ± 0.7% for HD 207129, whereas we derive A(Li) = 2.70 ± 0.04 and ^{6}Li/^{7}Li = 0.9% ± 1.4% for HD 95456. The correction for ^{6}Li/^{7}Li is estimated to be $\Delta q_{\rm 3DNLTE-1DLTE} = -1.1$% for HD 207129 and $\Delta q_{\rm 3DNLTE-1DLTE} = -1.9$% for HD 95456.

In the case of HD 95456, the 2σ detection of ^{6}Li in the 1D LTE analysis is turned into a clear non-detection after applying the 3D NLTE correction. In conclusion, we do not find significant amounts of ^{6}Li in either of the two stars.

Additionally, we studied the impact of two weak absorption lines (Si I, V I) on our ^{6}Li/^{7}Li measurements in HD 95456, and concluded that the Si I 670.8025 nm feature is the most critical blend for this analysis, confirming the result of Israelian et al. (2003).

Finally, we have demonstrated that a list of blend lines that are adjusted (like G09) by fine-tuning $\log gf$-values and wavelength positions to yield a perfect fit to the solar Li spectral region with a particular 1D model atmosphere cannot be expected to produce an equally good fit when employed unaltered for 3D modeling. For this reason, fitting 3D model spectra directly to observations may not always be the most desirable approach.

Acknowledgements. This work has made use of the VALD database, operated at Uppsala University, the Institute of Astronomy RAS in Moscow, and the University of Vienna. We thank the Leibniz-Association for supporting G.H. and A.M. through a SAW graduate school grant. JIGH acknowledges financial support from the Spanish ministry project MINECO AYA2014- 56359-P and from the Spanish Ministry of Economy and Competitiveness (MINECO) under the 2013 Ramón y Cajal program MINECO RYC-2013-14875. We thank János Bartus for creating the web page calculator. Finally, we thank the anonymous referee for his/her critical questions which helped us to improve the presentation of our results.

References

Adibekyan, V. Z., Sousa, S. G., Santos, N. C., et al. 2012, A&A, 545, A32
Asplund, M., Grevesse, N., Sauval, A. J., & Scott, P. 2009, ARA&A, 47, 481
Bensby, T., & Lind, K. 2018, A&A, 615, A151
Bertran de Lis, S., Delgado Mena, E., Adibekyan, V. Z., Santos, N. C., & Sousa, S. G. 2015, A&A, 576, A89
Caffau, E., Ludwig, H.-G., Steffen, M., et al. 2008, A&A, 488, 1031
Caffau, E., Ludwig, H.-G., Steffen, M., Freytag, B., & Bonifacio, P. 2011, Sol. Phys., 268, 255
Carlsson, M., Rutten, R. J., Bruls, J. H. M. J., & Shchukina, N. G. 1994, A&A, 288, 860
Cayrel, R., Steffen, M., Chand, H., et al. 2007, A&A, 473, L37
Cuntz, M., Saar, S. H., & Musielak, Z. E. 2000, ApJ, 533, L151
Delgado Mena, E., Bertrán de Lis, S., Adibekyan, V. Z., et al. 2015, A&A, 576, A69
Doyle, A. P., Davies, G. R., Smalley, B., Chaplin, W. J., & Elsworth, Y. 2014, MNRAS, 444, 3592
Dutra-Ferreira, L., Pasquini, L., Smiljanic, R., Porto de Mello, G. F., & Steffen, M. 2016, A&A, 585, A75
Forestini, M. 1994, A&A, 285, 473
Freytag, B., Steffen, M., & Dorch, B. 2002, Astron. Nachr., 323, 213
Freytag, B., Steffen, M., Ludwig, H.-G., et al. 2012, J. Comput. Phys., 231, 919
Ghezzi, L., Cunha, K., Smith, V. V., et al. 2009, ApJ, 698, 451 [G09]
Gomes da Silva, J., Santos, N. C., Boisse, I., Dumusque, X., & Lovis, C. 2014, A&A, 566, A66
Gray, D. F. 2005, The Observation and Analysis of Stellar Photospheres, 3rd edn. (Cambridge, UK: Cambridge Univ. Press)
Gustafsson, B., Edvardsson, B., Eriksson, K., et al. 2008, A&A, 486, 951
Howk, J. C., Lehner, N., Fields, B. D., & Mathews, G. J. 2012, Nature, 489, 121

Israelian, G., Santos, N. C., Mayor, M., & Rebolo, R. 2001, Nature, 411, 163
Israelian, G., Santos, N. C., Mayor, M., & Rebolo, R. 2003, A&A, 405, 753
Kawanomoto, S., Kajino, T., Aoki, W., et al. 2009, ApJ, 701, 1506
Klevas, J., Kučinskas, A., Steffen, M., Caffau, E., & Ludwig, H.-G. 2016, A&A, 586, A156
Kupka, F., Dubernet, M. L., & VAMDC Collaboration. 2011, Bal. Astron., 20, 503
Kurucz, R. 1993, ATLAS9 Stellar Atmosphere Programs and 2 km/s grid. Kurucz CD-ROM No. 13 (Cambridge, MA: Smithsonian Astrophysical Observatory), 13
Kurucz, R. L. 1995, ApJ, 452, 102
Kurucz, R. L. 2005, Mem. Soc. Astron. It. Sup., 8, 189
Lawler, J. E., Wood, M. P., Den Hartog, E. A., et al. 2014, ApJS, 215, 20
Lind, K., Asplund, M., & Barklem, P. S. 2009, A&A, 503, 541 [L2009]
Lind, K., Melendez, J., Asplund, M., Collet, R., & Magic, Z. 2013, A&A, 554, A96
Lodders, K. 2003, ApJ, 591, 1220
Ludwig, H.-G., Caffau, E., Steffen, M., et al. 2009, Mem. Soc. Astron. It., 80, 711
Mandell, A. M., Ge, J., & Murray, N. 2004, AJ, 127, 1147
Markwardt, C. B. 2009, in Astronomical Data Analysis Software and Systems XVIII, eds. D. A. Bohlender, D. Durand, & P. Dowler, ASP Conf. Ser., 411, 251
Mayor, M., Pepe, F., Queloz, D., et al. 2003, The Messenger, 114, 20
Meléndez, J., Bergemann, M., Cohen, J. G., et al. 2012, A&A, 543, A29 [M12]
Meneguzzi, M., Audouze, J., & Reeves, H. 1971, A&A, 15, 337
Montalbán, J., & Rebolo, R. 2002, A&A, 386, 1039
Montes, D., & Ramsey, L. W. 1998, A&A, 340, L5
Mott, A., Steffen, M., Caffau, E., Spada, F., & Strassmeier, K. G. 2017, A&A, 604, A44
Müller, E. A., Peytremann, E., & de La Reza, R. 1975, Sol. Phys., 41, 53
Pavlenko, Y. V., & Magazzu, A. 1996, A&A, 311, 961
Pavlenko, Y. V., Jenkins, J. S., Ivanyuk, O. M., et al. 2018, A&A, 611, A27
Pinsonneault, M. 1997, ARA&A, 35, 557
Prantzos, N. 2012, A&A, 542, A67
Prantzos, N., Casse, M., & Vangioni-Flam, E. 1993, ApJ, 403, 630
Proffitt, C. R., & Michaud, G. 1989, ApJ, 346, 976
Reddy, B. E., Lambert, D. L., Laws, C., Gonzalez, G., & Covey, K. 2002, MNRAS, 335, 1005
Sbordone, L., Bonifacio, P., Caffau, E., et al. 2010, A&A, 522, A26
Sneden, C. A., 1973, PhD Thesis, The University of Texas at Austin, USA
Sousa, S. G., Santos, N. C., Mayor, M., et al. 2008, A&A, 487, 373
Steffen, M., Cayrel, R., Bonifacio, P., Ludwig, H. G. & Caffau, E. 2010a, in Chemical Abundances in the Universe: Connecting First Stars to Planets, eds. K. Cunha, M. Spite, & B. Barbuy, IAU Symp., 265, 23
Steffen, M., Cayrel, R., Bonifacio, P., Ludwig, H. G., & Caffau, E. 2010b, in Light Elements in the Universe, eds. C. Charbonnel, M. Tosi, F. Primas, & C. Chiappini, IAU Symp., 268, 215
Steffen, M., Cayrel, R., Caffau, E., et al. 2012, Mem. Soc. Astron. It. Sup., 22, 152
Steffen, M., Prakapavičius, D., Caffau, E., et al. 2015, A&A, 583, A57
Strassmeier, K. G., Ilyin, I., & Steffen, M. 2018, A&A, 612, A44
Suárez-Andrés, L., Israelian, G., González Hernández, J. I., et al. 2017, A&A, 599, A96
Takeda, Y., & Kawanomoto, S. 2005, PASJ, 57, 45 [T2005]
Takeda, Y., & UeNo, S. 2017, PASJ, 69, 46
Talon, S., & Charbonnel, C. 2005, A&A, 440, 981
Thomas, D., Schramm, D. N., Olive, K. A., & Fields, B. D. 1993, ApJ, 406, 569
Tsantaki, M., Sousa, S. G., Adibekyan, V. Z., et al. 2013, A&A, 555, A150

Appendix A: 3D NLTE corrections for *A*(Li) and ^{6}Li/^{7}Li

Figures A.1–A.3 present the plots of 3D NLTE corrections $\Delta q_{\rm 3DNLTE-1DLTE}$ (left panels) and $\Delta A_{\rm 3DNLTE-1DLTE}$ (right panels) derived with line list K95 vs. the effective temperature for three metallicities of our 3D NLTE spectral grid ([Fe/H] = −1.0, −0.5 and 0.5, respectively). Figure A.4 shows the same 3D NLTE corrections derived with line list M12 for metallicity [Fe/H] = 0.0.

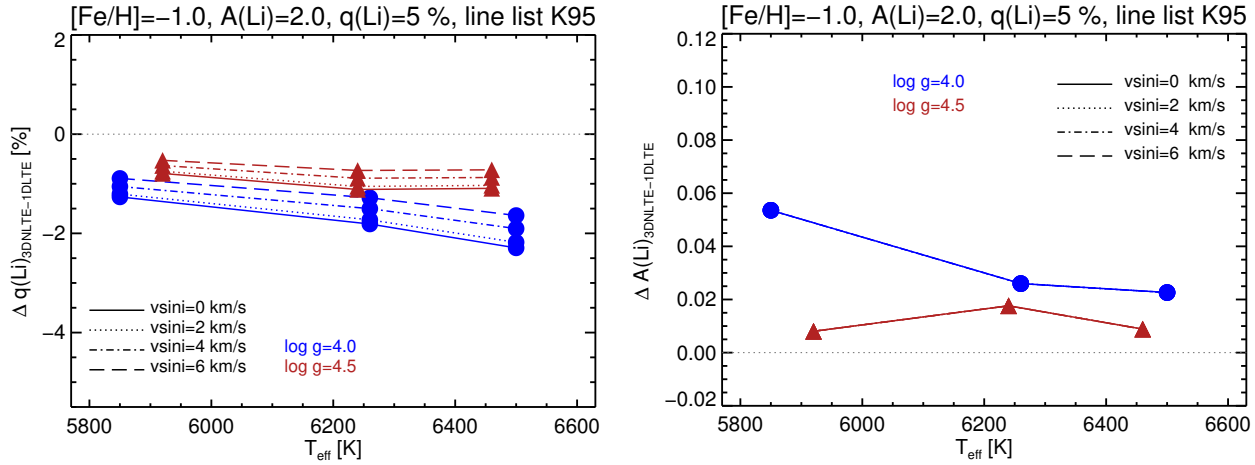

Fig. A.1. 3D NLTE corrections for ^{6}Li/^{7}Li (*left panel*) and *A*(Li) (*right panel*) vs. $T_{\rm eff}$ for [Fe/H] = −1.0, *A*(Li) = 2.0, *q*(Li) = 5%, derived with line list K95. The blue circles and the red triangles correspond to log *g* = 4.0 and log *g* = 4.5, respectively. The corrections for different $v \sin i$ values are connected with lines of different styles.

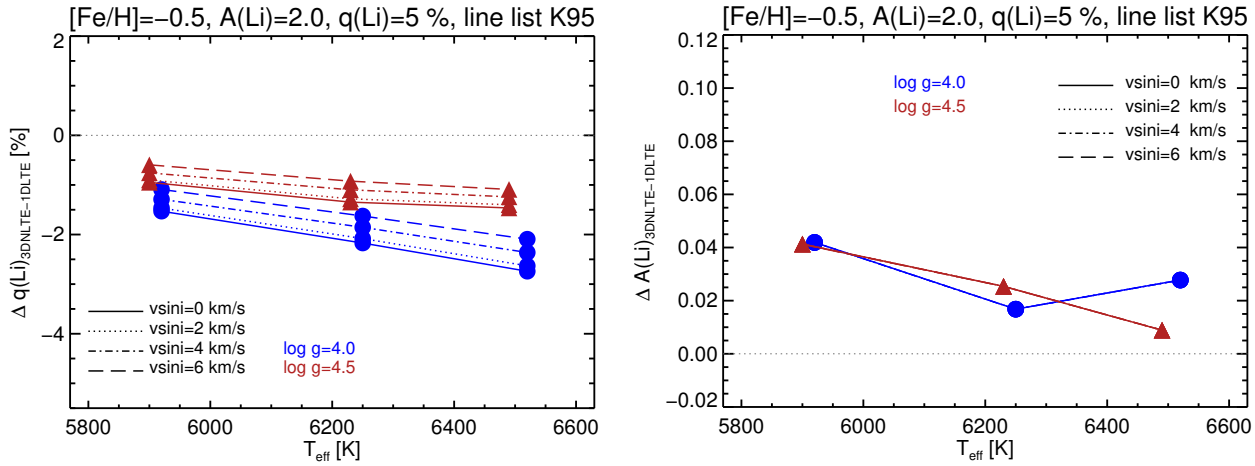

Fig. A.2. As Fig. A.1 but for [Fe/H] = −0.5.

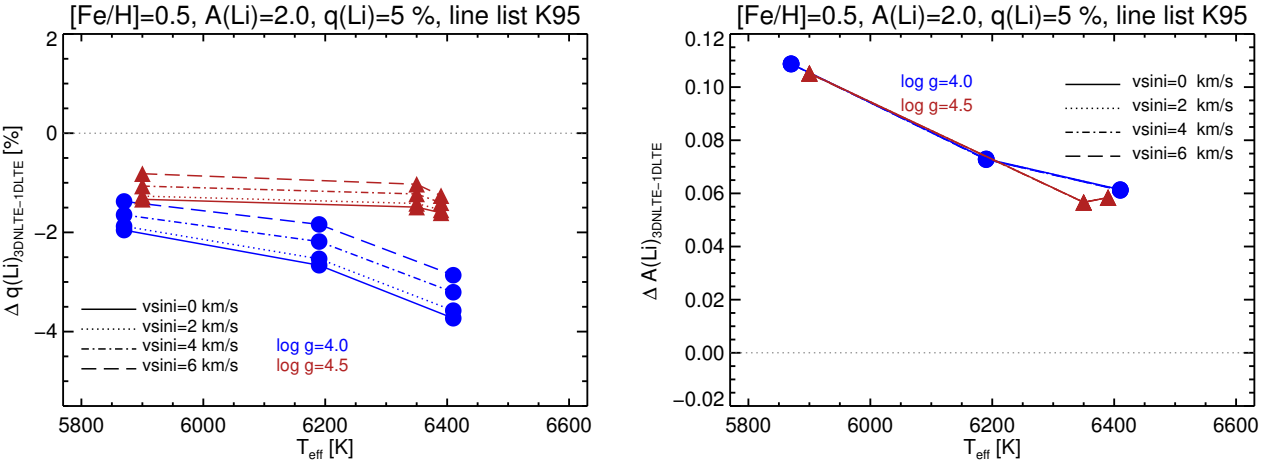

Fig. A.3. As Fig. A.1 but for [Fe/H] = +0.5.

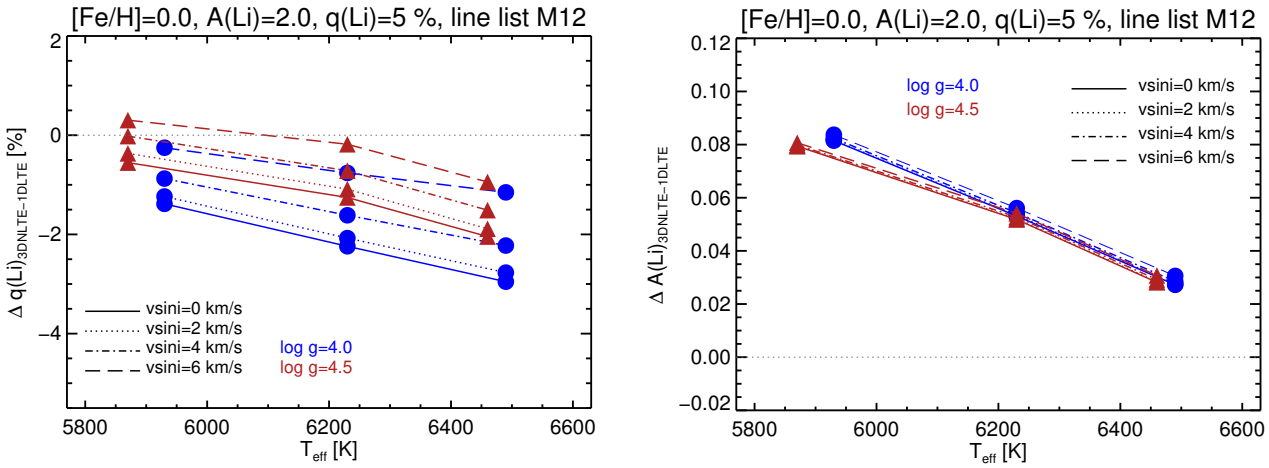

Fig. A.4. Same corrections as shown in Figs. A.1–A.3, but derived with line list M12 for [Fe/H] = 0.0.

Table B.1. Summary of 3D–1D fitting results.

Fit ID	Model	Line formation	Spectrum	A(Li) (dex)	q(Li) (%)	A(Si) (dex)	Δv (Si) (km s^{-1})	*FWHM* (km s^{-1})	Δv (km s^{-1})	χ^2
	3D	non-LTE	^{6}Li+^{7}Li	1.1000	0.00	0.0	–	0.500	0.0000	–
0	1D LHD	LTE	^{6}Li+^{7}Li	1.0003	0.83	0.0	–	4.031	−0.1877	17.2
	3D	LTE	Si	–	–	7.5500	–	0.500	0.0000	–
1	1D LHD	LTE	Si	–	–	7.5081	–	4.085	−0.3988	11.9
	3D	mixed	^{6}Li+^{7}Li+Si	1.1000	0.00	7.5500	0.00	0.500	0.0000	–
2a	1D LHD	LTE	^{6}Li+^{7}Li+Si	0.9945	−1.94	7.5500*	0.00*	4.268	−0.2280	2954.5
	3D	mixed	^{6}Li+^{7}Li+Si	1.1000	0.00	7.5500	0.00	0.500	0.0000	–
2b	1D LHD	LTE	^{6}Li+^{7}Li+Si	1.0029	1.89	7.5081*	0.00*	3.971	−0.2512	946.1
	3D	mixed	^{6}Li+^{7}Li+Si	1.1000	0.00	7.5500	0.00	0.500	0.0000	–
2c	1D LHD	LTE	^{6}Li+^{7}Li+Si	1.0001	0.80	7.5081*	−0.211*	4.058	−0.1891	41.18

Notes. Rows for 3D model specify the input parameters for the 3D spectrum synthesis; rows for 1D model give the results of the best fit (right part of the table), except numbers marked by an asterisk which are fixed input parameters. Δv (Si) (Col. 8) gives the artificial wavelength shift (converted to velocity) of the Si I line introduced in the line list for the 1D LTE spectrum synthesis. The relative quality of the fits can be judged by comparing their χ^2 (given on an arbitrary absolute scale).

Appendix B: Test case solar Li I + Si I blend

This numerical experiment is to demonstrate that the corrections $\Delta A_{\rm 3DNLTE-1DLTE}$ and $\Delta q_{\rm 3DNLTE-1DLTE}$ derived from fitting a 3D NLTE Li line profile with overlapping blend lines by a grid of corresponding 1D LTE spectra are very similar to the corrections obtained from fitting the pure Li 3D NLTE line profile with a grid of 1D LTE pure Li spectra, provided that the blend lines in the 1D spectrum synthesis are adjusted to correct for 3D effects.

We model the Li doublet in its full complexity, including all hyperfine structure levels of both ^{6}Li and ^{7}Li. The blends are represented by a single silicon line (Si I λ 670.8025 nm) which is known to have a critical influence on the derived ^{6}Li/^{7}Li (see Sect. 3.7). The Sun is a good test case since the solar Li abundance (A(Li) = 1.1) is at least ten times lower than in our target stars (A(Li) $\gtrsim$ 2.3) and hence the Si I line has an even larger impact on the Li profile.

As a first step, we fit the pure ^{7}Li 3D NLTE line profile computed with NLTE3D + Linfor3D from a 3D solar CO^{5}BOLD model with a grid of 1D LTE pure ^{6}Li+^{7}Li spectra based on a solar LHD model. The fitting parameters are (i) the Li abundance A(Li), (ii) the ^{6}Li/^{7}Li isotopic ratio q(Li), (iii) the width of a global Gaussian line broadening kernel FWHM, and (iv) a global Doppler shift Δv. The same procedure is repeated with the single Si I line, which is modeled in LTE both in 3D and in 1D, assuming the same atomic line parameters as in line list G09. Here the fitting parameters are A(Si), FWHM, and Δv. The best fit results are summarized in Table B.1 (Fit 0 and Fit 1). We notice that the 3D LTE abundance correction for the Si line is ΔA (Si) = +0.0419 dex, the absolute convective blue shift is $\Delta v = -0.399$ km s^{-1}, and the shift relative to Li is $\delta v = -0.399 + 0.188 = -0.211$ km s^{-1}.

In a second step, we fit the 3D composite spectrum of Li (NLTE) plus Si (LTE) with a grid of 1D LTE composite spectra covering a range in A(Li) and ^{6}Li/^{7}Li, but assuming the same fixed silicon abundance as in the 3D spectrum synthesis (A(Si) = 7.55). Under these constraints, the best fit is found for an isotopic ratio of ^{6}Li/^{7}Li = −1.9%. However, this fit (Fit 2a) is rather poor (see top panel of Fig. B.1 and Table B.1).

The fit can be improved if we reduce the silicon abundance by ΔA(Si) = −0.0419 dex, thus accounting for the 3D abundance corrections indicated by Fit 1. The resulting fit (Fit 2b) is significantly better and indicates ^{6}Li/^{7}Li = +1.9%. Still, the fit is clearly unsatisfactory (see middle panel of Fig. B.1).

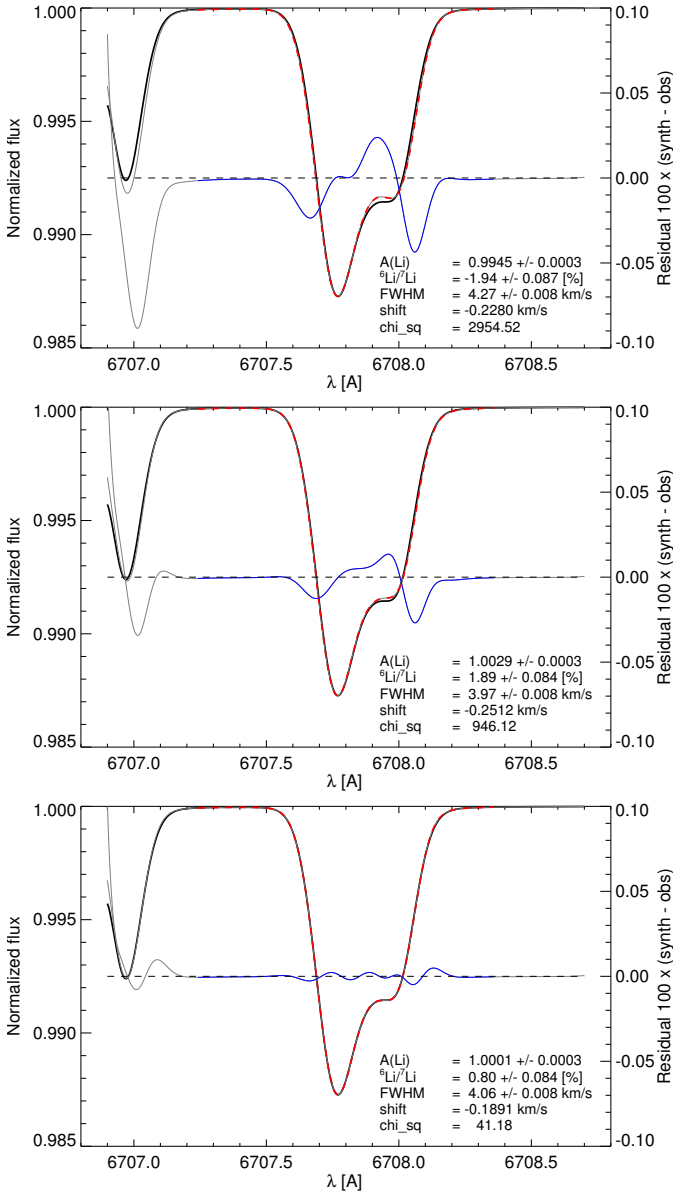

Fig. B.1. Best 1D fits (dashed line) to the 3D composite ^{7}Li (NLTE) + Si (LTE) synthetic solar line profile (black solid line) achieved with different grids of 1D LTE ^{6}Li+^{7}Li+Si profiles. *From top to bottom*: cases 2a, 2b, and 2c (see text and Table B.1 for details). The right *y*-axis defines the scale of the residuals (thin blue line).

A much better fit can be obtained if we allow in addition for a wavelength shift of the Si line of $\delta v = -0.211$ km s^{-1} in the 1D spectrum synthesis to compensate for the convective blue shift of Si relative to Li. The solution for this setup (Fit 2c, shown in the lower panel of Fig. B.1) is very acceptable. The derived ^{6}Li/^{7}Li is now essentially the same as the one indicated by the analysis of the pure Li case (cf. Fit 0 and Fit 2c in Table B.1).

The conclusion of this numerical experiment is that a list of blend lines, adjusted (like G09) by fine-tuning $\log gf$-values and wavelength positions to yield a perfect fit to the solar Li spectral region with a particular 1D model atmosphere, cannot be expected to produce an equally good fit when employed unaltered for 3D modeling. It is therefore not surprising that the 3D analysis of the solar Li region with unmodified line list G09 produces a fit of somewhat inferior quality compared to the original 1D analysis by Ghezzi et al. (2009), and leads to somewhat different results for ^{6}Li/^{7}Li. Consistent results in 3D can only be achieved if line list G09 is adjusted for 3D effects. In this case, we expect that ^{6}Li/^{7}Li (3D) $\approx$ ^{6}Li/^{7}Li (1D)-0.8% (cf. Appendix C).

Appendix C: Fitting the solar Li I λ 670.8 nm region with 1D LHD and 3D CO^{5}BOLD synthetic spectra

In this Appendix, we derive the solar lithium abundance and ^{6}Li/^{7}Li by fitting the Li I λ 670.8 nm spectral region of solar flux spectrum (Kurucz 2005) with synthetic spectra computed from a solar 1D LHD model ($T_{\rm eff} = 5780$ K, $\log g = 4.44$, $V_{\rm micro} = 1.0$ km s^{-1}, $\alpha_{\rm MLT} = 1.0$) and a 3D CO^{5}BOLD model atmosphere, respectively. The purpose of this investigation is to test the expected relation between the 1D and the 3D results.

In both cases, the spectrum synthesis is performed with Linfor3D, applying a fixed rotational broadening of $v \sin i = 1.8$ km s^{-1} in the flux convolution approximation. As before, the Li doublet includes all hyperfine structure levels of both ^{6}Li and ^{7}Li and is treated in NLTE (LTE) when computing the grid of spectra from the 3D (1D LHD) models.

The grid of 1D LHD spectra is computed with line list G09. The fitting of the solar flux spectrum with this grid follows the same methodology as the fitting with the ATLAS/MOOG spectra described in Sect. 3.8. For a fixed continuum level, the basic fitting parameters are (i) the Li abundance A(Li), (ii) the ^{6}Li/^{7}Li isotopic ratio q(Li), (iii) the width of a global Gaussian line broadening kernel FWHM, and (iv) a global Doppler shift Δv. In addition, we allow for small adjustments of the strengths (abundances or $\log gf$ values) of the CN, Fe I, Si I, and V I lines to further optimize the fit.

In *Case I*, we fix the continuum at the same level as for the best fit with the ATLAS/MOOG spectra (Case C, Fig. 8), $c_1 = 0.9977$ (relative to the continuum placement of the solar flux atlas). The best fit with our grid of 1D LHD synthetic spectra if found for A(Li) = 0.94 and q(Li) = 0.69% (see Fig. C.1). These results can be compared to those of Case C, A(Li) = 0.98 and q(Li) = 0.71%. While the derived ^{6}Li/^{7}Li is practically identical, the lithium abundance indicated by the LHD fit is slightly lower. This must be related to slight differences in the temperature stratification of the solar LHD model relative to the ATLAS9 model.

Next we fit the observed spectrum with a grid of synthetic spectra derived from the CO^{5}BOLD 3D solar atmosphere, now treating the Li doublet in NLTE. Adopting the same continuum level as for the 1D fitting, we try out different assumptions about the chemical abundances and the wavelengths of the blend lines.

In *Case Ia*, we use the same line list (G09) as in *Case I* together with the same 1D-optimized individual abundances obtained from the best fit with the 1D LHD spectra. Under these constraints, the best fit requires A(Li) = 1.05 and q(Li) = 1.86%. As expected, the fit is rather poor (see Fig. C.2, top panel).

At the next stage (*Case Ib*), we adjust the strengths of the CN, Fe, Si, and V blend lines according to the 3D–1D abundance corrections inferred from fitting the 3D synthetic line profiles of the individual blend lines by a grid of corresponding 1D spectra of different abundance, as described for the Li and Si lines in Appendix B. The fit with these adjusted abundances is shown in Fig. C.2 (middle panel), indicating A(Li) = 1.04 and a strongly negative ^{6}Li/^{7}Li of less than -2%. While the fit is generally improved with respect to *Case Ia*, the Fe+CN blend at λ 670.74 nm is by far not reproduced to the level of precision achieved with the 1D LHD fit (cf. Fig. C.1).

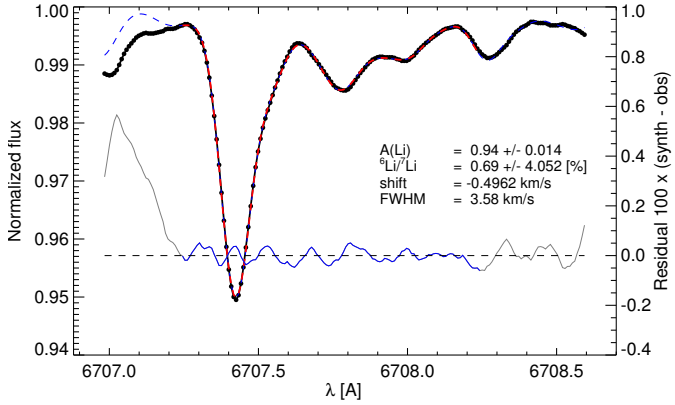

Fig. C.1. The best fitting 1D LTE LHD spectrum (red dashed line) superimposed on the solar flux spectrum of Kurucz (2005; black dots), fixing the continuum level at 0.9977 (relative to the continuum placement of the flux atlas), and using line list G09 with slight adjustments in the strengths of the CN, Fe, Si, and V lines (*Case I*, Table C.1) The right *y*-axis defines the scale of the residuals (thin blue line).

A 3D fit of comparable quality can be accomplished by readjusting the rest wavelengths of the main blend components according to their differential convective Doppler shifts. The latter are again deduced from fitting the synthetic 3D line profiles by their 1D counterparts, as described for the Li and Si lines in Appendix B. In *Case Ic*, we applied both these "theoretical" convective wavelength shifts and related abundance corrections to the CN, Fe, Si, and V blend lines. Indeed, the applied wavelength shifts[3] lead to a dramatic improvement of the fit (see Fig. C.2), bottom panel). Now the best solution is found for $A(\mathrm{Li}) = 1.05$ and $q(\mathrm{Li}) = -0.18\%$. We notice that the $^6\mathrm{Li}/^7\mathrm{Li}$ found from this fine-tuned 3D fit is now in very good agreement with the result from the LHD fit after application of the $\Delta q_{\mathrm{3DNLTE-1DLTE}}$ correction ($0.69 - 0.83 = -0.14\%$).

We performed the same exercise for a different continuum level, $c_1 = 0.9980$ (*Case II*), which corresponds closely to the continuum placement adopted for the analysis of the PEPSI spectrum in Strassmeier et al. (2018). We verified (*Case IIx*) that we obtain very similar results when adopting their set of abundances: $A(\mathrm{Li}) = 1.09$ and $q(\mathrm{Li}) = 1.77 \pm 2.2\%$, compared to $A(\mathrm{Li}) = 1.09$ and $q(\mathrm{Li}) = 1.44 \pm 1.6\%$ in Strassmeier et al. (2018). Quantitatively, the two series of fits at slightly different continuum levels show a systematic offset in the absolute values of $A(\mathrm{Li})$ and $q(\mathrm{Li})$, but otherwise follow the same qualitative trends and lead to the same conclusions. Details of all fits discussed above can be found in Table C.1.

In summary, the fits of the solar spectrum by grids of 1D LHD and 3D CO^{5}BOLD synthetic spectra computed with the full G09 line list justify our definition of the 3D NLTE corrections for $A(\mathrm{Li})$ and $q(\mathrm{Li})$ based on the comparison of 3D NLTE and 1D LTE Li-only line profiles. This conclusion is not limited to the solar case but should apply even more to the target stars of this paper, where a strong lithium feature dominates over relatively weak blend lines.

We chose the Sun for demonstration because all involved spectral lines are weak and therefore the combined spectrum may be constructed by linear superposition of the individual components. The presence of stronger lines would require a full spectrum synthesis of the complete spectrum for each individual configuration. Under these conditions, a fine-tuned 3D (NLTE) fit to the observed spectra of our target stars would be next to impossible. However, the exercise presented in this Appendix also strongly suggests that using 3D model spectra directly for the fitting is not really the most desirable approach since it requires non-trivial adjustments in the line lists that are fine-tuned by 1D methods.

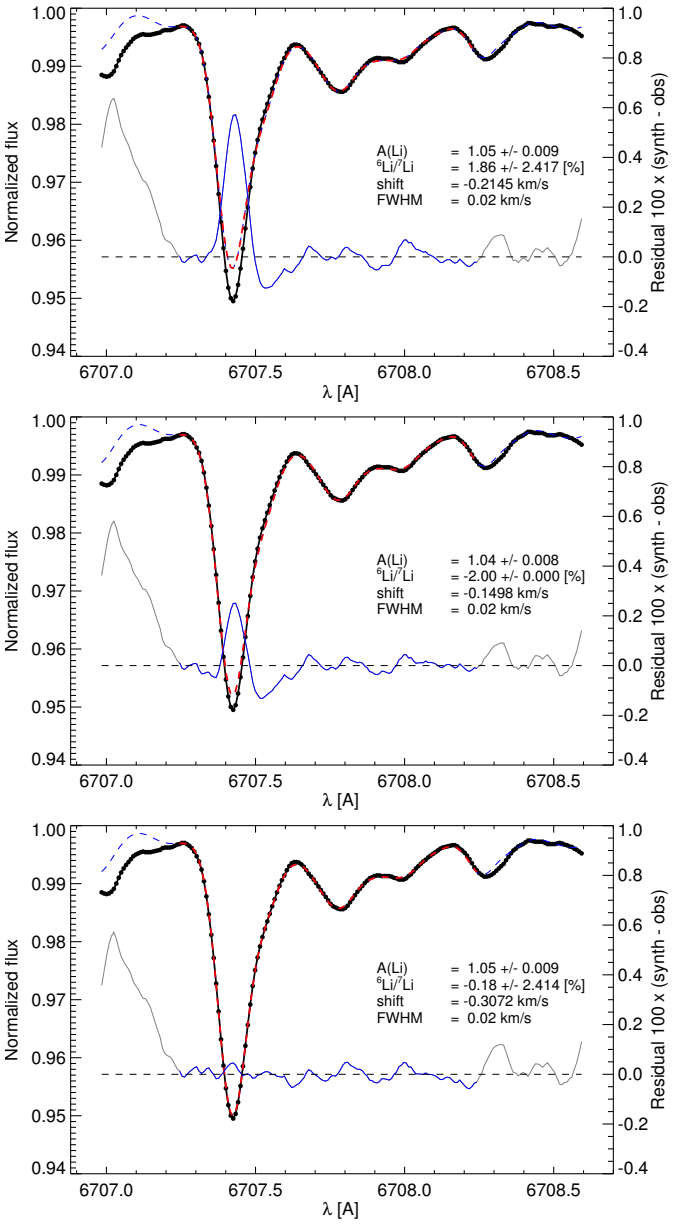

Fig. C.2. Best fits of the solar flux spectrum of Kurucz (2005; black dots) with different sets of 3D NLTE CO^{5}BOLD spectra (red dashed line), adopting the same continuum level as in Fig. C.1. *From top to bottom*: *Cases IIa, IIb*, and *IIc* are all based on line list G09, but assume different chemical abundances and rest wavelengths of the blend lines (see text and Table C.1 for details). The right *y*-axis defines the scale of the residuals (thin blue line).

[3] The asymmetric 3D profile of the Fe line at λ 670.74 nm is represented by two components in 1D.

Table C.1. Summary of the results of fitting the Li region of the solar flux spectrum (Kurucz 2005) with 1D LHD and 3D CO^{5}BOLD synthetic spectra.

Fit ID	Model	Continuum level	Abundances	Wavelengths	A(Li) (dex)	q(Li) (%)	χ^2
I	1D LHD	0.9977	adjusted	G09	0.94	0.69	8.2
Ia	3D CO^{5}BOLD	0.9977	as Fit I	G09	1.05	1.86	251.3
Ib	3D CO^{5}BOLD	0.9977	Fit I +ΔA	G09	1.04	<−2.0	53.6
Ic	3D CO^{5}BOLD	0.9977	Fit I +ΔA	G09 +$\Delta\lambda$	1.05	−0.18	7.3
II	1D LHD	0.9980	adjusted	G09	0.96	1.67	7.9
IIa	3D CO^{5}BOLD	0.9980	as Fit II	G09	1.06	2.88	247.3
IIb	3D CO^{5}BOLD	0.9980	Fit II +ΔA	G09	1.06	−0.89	54.0
IIc	3D CO^{5}BOLD	0.9980	Fit II +ΔA	G09 +$\Delta\lambda$	1.06	0.88	6.1
IIx	3D CO^{5}BOLD	0.9980	SIS18	G09	1.09	1.77	29.5

Notes. Column (4): ΔA symbolizes the individual 3D abundance corrections; "SIS18" indicates the same abundances as used in Strassmeier et al. (2018). Column (5): G09 denotes the line list of Ghezzi et al. (2009), $\Delta\lambda$ symbolizes the individual convective line shifts. The relative quality of the fits can be judged by comparing their χ^2 (given on a common absolute scale).